Centrosomal Enrichment and Proteasomal Degradation of SYS-1/β-catenin Requires the Microtubule Motor Dynein

Joshua W. Thompson, Maria F. Valdes Michel, Bryan T. Phillips

Abstract

The *C. elegans* Wnt/β-catenin Asymmetry (WβA) pathway utilizes asymmetric regulation of SYS-1/β-catenin and POP-1/TCF coactivators. WβA differentially regulates gene expression during cell fate decisions, specifically by asymmetric localization of determinants in mother cells to produce daughters biased towards their appropriate cell fate. Despite the induction of asymmetry, β-catenin localizes symmetrically to mitotic centrosomes in both mammals and *C. elegans*. Due to the mitosis-specific localization of SYS-1 to centrosomes and enrichment of SYS-1 at kinetochore microtubules when SYS-1 centrosomal loading is disrupted, we investigated active trafficking in SYS-1 centrosomal localization. Here, we demonstrate that trafficking by microtubule motor dynein is required to maintain SYS-1 centrosomal enrichment, by dynein RNAi-mediated decreases in SYS-1 centrosomal enrichment and by temperature-sensitive allele of the dynein heavy chain. Conversely, we observe depletion of microtubules by Nocodazole treatment or RNAi of dynein-proteasome adapter ECPS-1 exhibits increased centrosomal enrichment of SYS-1. Moreover, disruptions to SYS-1 or negative regulator microtubule trafficking are sufficient to significantly exacerbate SYS-1 dependent cell fate misspecifications. We propose a model whereby retrograde microtubule-mediated trafficking enables SYS-1 enrichment at centrosomes, enhancing its eventual proteasomal degradation. These studies support the link between centrosomal localization and enhancement of proteasomal degradation, particularly for proteins not generally considered 'centrosomal'.

Keywords

Development, Wnt, β-catenin, microtubule, ECM29, dynein, proteasome, trafficking, elegans, asymmetry, cell cycle, robustness

30 **Introduction**

31 During metazoan development, cells must robustly respond to and integrate multiple signaling
32 pathways to appropriately specify and populate tissues. This is of further importance in the developing
33 embryo, where cell division rapidly alternates between S-phase and mitosis while simultaneously
34 specifying tissues and entire germ layers (Pintard and Bowerman 2019). As such, the cell's response to
35 these signals and the subsequent establishment of asymmetry often begins before asymmetric daughter
36 cells are even 'born' via an asymmetric cell division (ACD) (Sunchu and Cabernard 2020; Juanes, 2020;
37 Fuchs and Chen, 2013; Gómez-López, Petrisch et al 2014). Among the signaling pathways utilized in
38 development is Wnt/β-catenin signaling, wherein the binding of Wnt ligands disrupts β-catenin
39 degradation via dismantling an intracellular destruction complex. This effectively stabilizes β-catenin,
40 enabling it to activate target genes with transcriptional activator TCF/LEF (Nusse and Clevers 2017).
41 Wnt/β-catenin signaling is specialized in its ability to regulate both polarity and proliferation – enabling
42 developing organisms to orient and expand tissues simultaneously for appropriate size and morphology
43 (Loh et al 2016). Due to its role in both proliferation and polarity, Wnt/β-catenin signaling is readily
44 adaptable to the adult organism throughout development.

45 Wnt/β-catenin is particularly well adapted to the organization of a patterned stem cell niche for
46 proliferative tissue maintenance (Pinto, Clevers et al 2003; Reilein, Kalderon et al 2017). However, this
47 function in adult tissue homeostasis also associates deleterious dysregulation of Wnt/β-catenin signaling
48 with disease states. Throughout transduction of the Wnt signal are proteins vulnerable to oncogenic
49 mutation (Yang, yen 2011; Zhunussova, Djansugurova et al 2019; Liu, Thibodeau et al 2000). However,
50 these often affect their tumorigenicity via dysregulation of the pathway effector β-catenin, which can
51 promote proliferation via over-and mis-expression of targets like Cyclin D1 and cMyc (Niehrs, Acebron
52 2012; He, Kinzler et al 1998; Shtutman, Ben-Ze'ev et al 1999; Tetsu and McCormick, 1999). Moreover, β-

53 catenin is a bifunctional protein in mammalian systems. That is, it is distributed between the previously
54 described signaling role while also maintaining cell-cell adhesion at adherens junctions (Niehrs, Acebron
55 2012; Reya, Clevers 2005), where it facilitates the interaction between membrane protein E-cadherin
56 and the cytoskeleton. The combination of these roles for β-catenin makes it an attractive target for
57 studying tumorigenesis, both due to hyperproliferative phenotypes and ease of metastasis. However,
58 the dual functions can also lead to confounding pleiotropic phenotypes after manipulation of β-catenin
59 activity (Reya, Clevers 2005; Tejpar, Alman et al 1999; Geyer, Reis-Filho et al 2011).

60 Unlike β-catenin in the canonically described Wnt signaling pathway, *C. elegans* has distributed
61 the adhesive and signaling roles across its four β-catenins (Sawa, 2012). Here we focus specifically on
62 the *C. elegans* β-catenin SYS-1 for its role as a transcriptional co-activator in a modified Wnt/β-cat
63 signaling pathway, the Wnt/β-catenin Asymmetry pathway(WβA) (Phillips, Kimble et al 2007). The WβA
64 pathway is a specialized application of the more basic Wnt signaling paradigm, wherein regulation of the
65 co-activator SYS-1 (β-catenin) modulates the activity of transcription factor POP-1 (TCF), during
66 asymmetric cell division (Baldwin and Phillips 2018, Lam and Phillips 2017). Mother cells undergoing a
67 WβA-driven division polarize components of the Wnt signaling pathway along the axis of the division –
68 distributing positive regulators of a Wnt response, the Frizzled receptor and downstream effector
69 Disheveled, to the signaled pole of the cell, and negative regulators, members of the β-Catenin
70 destruction complex APC and Axin, to the unsignaled pole (Baldwin and Phillips 2014; Baldwin, Phillips et
71 al 2016; Sugioka, Sawa et al 2011; Mizumoto and Sawa, 2007). Daughter cells in such a division
72 therefore inherit Wnt signaling components that bias them toward their appropriate cell fate. Contrary
73 to its known role asymmetrically activating Wnt target genes, SYS-1 (and indeed, mammalian β-catenin
74 (Mbom, Barth et al 2014; Vora, Phillips et al 2020)), unexpectedly localizes symmetrically to mother cell
75 mitotic centrosomes (Phillips, Kimble et al 2007; Huang, Lin et al 2007; Vora and Phillips 2015).

76 Previous work has demonstrated that mother cell centrosomal localization of SYS-1 limits SYS-1
77 levels in daughter cells in a proteasome dependent manner (Vora and Phillips 2015). Differential
78 localization of the proteasome during the cell cycle (Amsterdam, Baumeister et al 1993), as well as
79 interactor-specific localization of the proteasome for intracellular structuring (Baldin, Coux et al 2008),
80 suggest that proteasome regulation, localization, and activity are interdependent. Proteasomal subunits
81 have specifically been shown to co-sediment with centrosomal proteins and perinuclear inclusions,
82 indicative of centrosomal localization (Wigley, Thomas et al 1999; Wojcik, DeMartino 2003). Similarly,
83 turnover of the SYS-1 mobile fraction at mitotic centrosomes is enhanced by RPT-4 proteasomal activity
84 (Vora and Phillips 2015). When the localization of SYS-1 to centrosomes is reduced by *rsa-2(RNAi)*,
85 resultant daughter cells retain 40% additional SYS-1 protein. Perhaps, then, the centrosome is a region
86 where SYS-1 regulatory interactions are concentrated to coordinate its retention and effect on cell fate
87 during mitosis.

88 The directionality and temporal specificity of SYS-1 enrichment at only mitotic centrosomes
89 implied that a more active localization mechanism might be at work, as compared to a passive diffusion-
90 capture mechanism. SYS-1 motility is most directly demonstrated in that the cell maintains a
91 proteasome-dependent, 100% mobile population of centrosomal SYS-1, which is recycled within 120
92 seconds (Vora and Phillips 2015). Cells appear to maintain robust localization of SYS-1 to the mitotic
93 centrosome, while the interphase centrosome remains undetectable via SYS-1 fluorescence (Vora and
94 Phillips 2015). However, the mechanism of such temporally specific SYS-1 centrosomal localization is
95 unknown. Several observations indicate that cells utilize the microtubule cytoskeletal network for rapid
96 and directional regulation of specific cargo to precise locales, including: that dynein conditionally traffics
97 transcription factors due to neuronal injury or signaling status, (Ben-Yaakov, Fainzilber et al 2012;
98 Mikenberg, Kaltschmidt et al 2007) and that dynein more generally can enrich endocytic recycling
99 components around the Microtubule Organizing Center (MTOC) (Horgan, Mccaffrey et al 2011) or be

100 sufficient to prevent pathogenic accumulation of RNA binding proteins (Deshiumaru, Tsuboi et al 2021).
101 Therefore, we hypothesized that the role of the mitotic centrosome as an MTOC could facilitate the
102 rapid transport of SYS-1 to the pericentriolar material specifically in dividing cells.

103 The rapid and cell cycle phase-specific enrichment of SYS-1 at the centrosome suggests that it
104 may also depend on active transport. Further, accumulation at a highly active MTOC like the mitotic
105 centrosome is most likely accomplished by the microtubule minus end-directed dynein motor complex
106 (Vora and Phillips 2015; Priyanga, Bhaka-Guha et al 2021). The dynein motor is a multi-subunit complex
107 composed of a pair of ATP-ase, microtubule-binding heavy chains responsible for the force-generating
108 steps of the motor, and a variable complement of smaller light, intermediate, and accessory chains that
109 alter the cargo binding or processivity of the motor (Reck-Peterson, Carter et al 2018; Jha and Surrey
110 2015). The dynein motor is multifunctional - it provides pulling forces, positions organelles, and can
111 mediate rapid and conditional movement of proteins and RNAs (Carminati and Stearns 1997; Woźniak,
112 Allan et al 2009; Harada, Hirokawa et al 1998; Hanz, Fainzilber et al 2003; Bullock and Ish-Horowicz
113 2001). For example, injured rat axons have demonstrated a dynein intermediate chain-dependent
114 nuclear localization and coimmunoprecipitation of the transcription factor STAT3, in order to
115 appropriately adopt an injury-dependent transcriptional response (Ben-Yaakov, Fainzilber et al 2012).
116 Dynein specifically is the motor complex most often directed towards the MTOC and is known to be
117 active during mitosis (Jha and Surrey 2015). Therefore, we investigated dynein-dependent trafficking as
118 an ideal mechanism for SYS-1 localization to the MTOC mitotic centrosomes.

119 Here we demonstrate that microtubules and minus-end microtubule-mediated trafficking are
120 required for the centrosomal recruitment of both SYS-1 and the negative regulators responsible for its
121 regulation there. We evaluate the extent to which SYS-1 utilizes dynein-mediated trafficking to
122 accumulate at centrosomes. Using both long- and short-term disruptions to dynein and microtubule-
123 mediated trafficking to evaluate SYS-1 localization and SYS-1-dependent cellular activity up to and

124 including cell fate changes, we demonstrate that SYS-1 and its negative regulators both require
125 microtubule-mediated trafficking for appropriate regulation of SYS-1. Together, these data characterize
126 a system for enhancing the robustness of the WβA signaling pathway by maintaining consistent
127 interaction of SYS-1 with negative regulators at the mitotic centrosome.

128 **Results**

129 **SYS-1 Overexpression and Centrosomal Uncoupling Increases SYS-1 Localization to Regions of Dynein**
130 **Enrichment**

131 To test the role of microtubule-mediated trafficking in SYS-1 centrosomal localization, we investigated
132 what trafficking mechanisms are necessary for SYS-1 regulation. We compared fluorescently tagged
133 SYS-1 protein localization to that of MT trafficking components. Of most interest was the cytoplasmic
134 dynein motor complex, since its components have been shown to localize to mitotic centrosomes,
135 kinetochore microtubules, and cortically across species (Schmidt, Van den Heuvel et al 2017; Tame,
136 Medema et al 2014). The dynein localization pattern corresponded to that of GFP::SYS-1 to cortical and
137 microtubule dense regions. Moreover, kinetochore and cortical localization was more common upon
138 centrosomal uncoupling, complete loss of visible enrichment of centrosomal SYS-1, by RNAi depletion of
139 the spindle assembly and scaffolding protein RSA-2(Fig. 1A).

140 While GFP::SYS-1 has been observed at mitotic centrosomes in many dividing cells throughout
141 development, localization to these cortical and kinetochore 'secondary' sites is uncommon
142 (accumulation at either or both of these sites occurring in 34.5% of embryos) in untreated embryos but
143 the frequency of this localization approximately doubles, to 69.1%, with *rsa-2(RNAi)* (Fig.1A). Uncoupling
144 SYS-1 protein from the centrosome by *rsa-2(RNAi)*, thereby decreasing processing of the protein, allows
145 us to more frequently observe SYS-1 at sites of dynein localization (Vora and Phillips 2015, Vora and
146 Phillips 2017)(Fig.1A). Localization to kinetochore microtubules, cortex, and the MTOC centrosome

147 therefore suggests that SYS-1 may be a cargo of the comparably localized dynein and kinesin
148 microtubule motors (Ferenz, Wadsworth et al 2010; Schmidt, Van den Heuvel et al 2017).

149

150 **Knockdown of Dynein Complex Subunits Reduces SYS-1 Centrosomal Localization**

151 Given the observation that SYS-1 localizes to cortical and kinetochore sites that also exhibit
152 enrichment for microtubule motors, we investigated a functional role for microtubule-mediated
153 trafficking in SYS-1 localization. We began by performing an RNAi screen against various components of
154 the dynein motor complex and associated proteins, eventually expanding outward to additional motors
155 and microtubule-affecting proteins (Fig. S1). Specifically, by RNAi depletion of these microtubule
156 trafficking proteins, we assayed the centrosomal enrichment of GFP::SYS-1. We expected depletion of
157 transport proteins that play a role in SYS-1 centrosomal transport to be defective in the maintenance of
158 SYS-1 centrosomal enrichment when SYS-1 centrosomal clearance was otherwise unaffected. In order to
159 evaluate the centrosome-specific enrichment of SYS-1, we considered two ways of comparing the extent
160 of fluorescently-tagged SYS-1 localization to centrosomes: 1) the centrosomal enrichment index
161 (CEI)(similar to that described in Gao, Smith et al 2017), the centrosomal fluorescence intensity adjusted
162 by subtraction of the background cytoplasmic fluorescent intensity of the surrounding cell, to control for
163 backgrounds that may pleiotropically influence SYS-1 expression, and 2) the SYS-1 CEI evaluated as a
164 ratio to the same enrichment factor of representative Peri Centriolar Material (PCM) factor γ-tubulin
165 (Tubulin Enrichment Index, or TEI) , to avoid false positives via defects in PCM maturation (CEI/TEI) (Fig.
166 1B-B''). We then compared these centrosomal enrichment metrics to those seen in established *rsa-*
167 *2(RNAi)* centrosomal uncoupling.

168 As expected, depletion of several dynein subunit knockdowns presented pleiotropic and
169 deleterious effects, including oogenesis and early patterning defects which precluded our SYS-1

170 localization assay. We therefore treated animals with partial RNAi knockdowns by commencing RNAi
171 feeding 12-24 hours before imaging as necessary, based on the phenotypic severity. While no
172 treatment disrupted SYS-1 centrosomal levels as severely as *rsa-2(RNAi)*, we did observe several
173 statistically significant decreases in centrosomal SYS-1 enrichment (Fig. 2C – C', Fig. S1). Furthermore,
174 while the total population of some treatments displayed only an intermediate mean loss of SYS-1
175 enrichment, the distribution of SYS-1 CEI values observed in dynein subunit knockdowns extends from
176 wild-type to an *rsa-2(RNAi)*-like disruption (e.g., Fig. 2 Supplement 1). Dynein knockdown-induced
177 decreases in SYS-1 CEI or CEI/TEI are masked somewhat in the population average by their broad range
178 in phenotype and/or RNAi penetrance (Fig. 1C-C', Fig S2). Most notably, *dlc-1(RNAi)* and *dylt-1(RNAi)*
179 each exhibit a significant reduction in centrosomal SYS-1 localization disproportionately larger than the
180 effect on γ-Tubulin. Loss of centrosomal SYS-1 enrichment was specifically more visible in a transgene
181 driven by the endogenous SYS-1 promoter (P_{sys-1}::VENUS::SYS-1), as compared to SYS-1 driven by the
182 stronger *pie-1* promoter (P_{pie-1}::GFP::SYS-1) (Fid 2C-C').

183 While we observed dynein-dependent decreases in SYS-1 localization, this could be because of
184 changes in the RSA-2 centrosomal scaffold, which is responsible for capturing SYS-1 at mitotic
185 centrosomes (Vora and Phillips 2015, Schlaitz, Hyman et al 2007). While some dynein subunits did show
186 slight decreases in centrosomal GFP::RSA-2 – 16% reduction in *dlc-1(RNAi)* embryos and 14% in *dylt-*
187 *1(RNAi)* embryos. Embryos depleted of DLC-1 by RNAi exhibit double this effect on SYS-1 localization,
188 with 39% and 42% reductions in Psys-1::VENUS::SYS-1 CEI and CEI/TEI, respectively. DYLT-1 depletion
189 exhibited a similar 14% decrease in CEI alone, but a 39% decrease in CEI/TEI. Both knockdowns suggest
190 that tagged SYS-1 is disproportionately removed from centrosomes in dynein knockdowns (Fig. S3)

191 These data suggest that dynein does have a role in the localization of SYS-1 to centrosomes, but
192 redundancy between components of the dynein motor or between the dynein motor and other
193 processes may limit the effect any one subunit has on SYS-1 localization. Alternately, while mutants are

194 often severely deleterious, variability of RNAi efficacy may have resulted in incomplete depletion of SYS-
195 1 relevant dynein subunits. Similarly, the pleiotropic effects of dynein depletion may also have
196 superseded effects on SYS-1 localization, leading to the evaluation of only partial knockdowns. In order
197 to address these issues, we investigated the role of the dynein motor in SYS-1 localization at a more
198 precise temporal resolution via conditional dynein disruption.

199 **Temporally Restricted Dynein Loss of Function Reveals Dynein Requirement for Centrosomal SYS-1**
200 **Accumulation.**

201 While our screen showed that dynein knockdown results in significant reduction of centrosomal SYS-1,
202 with rare individuals exhibiting *rsa-2(RNAi)*-like loss of centrosomal SYS-1 accumulation, we were unable
203 to completely recreate a population exhibiting consistently severe disruption to SYS-1 CEI. To distinguish
204 the variety in effect on SYS-1 localization effects between functional redundancies limiting the effects of
205 dynein depletion and the confounding deleterious effects described above, we utilized a temperature
206 sensitive allele of the cytoplasmic dynein heavy chain, *dhc-1(or195ts),* to conditionally inactivate the
207 cytoplasmic dynein heavy chain. This allele, identified in the Bowerman lab, introduces a lesion to the
208 microtubule binding stalk of DHC-1. This lesion renders the motor slightly hypomorphic at the
209 permissive 15°C (with 91% of embryos remaining viable and fertile) but undergo complete mitotic
210 spindle collapse as little as 30 seconds upon upshift, suggesting that DHC-1 motor function has been
211 nearly completely ablated (O'rourke, Bowerman et al. 2007).

212 Therefore, we expected that combining the *dhc-1(ts)* allele with fluorescently tagged SYS-1
213 would allow us to examine a more penetrant dynein knockdown. Notably, this allowed us to overcome
214 both redundancy between dynein accessory chains in SYS-1 trafficking as well as pleiotropic effects of
215 dynein depletion that preclude the observation of mitotic centrosomal SYS-1 (Fig. 2A). As described
216 above, we compared the CEI of $P_{sys\text{-}1}$:VENUS::SYS-1 (VENUS::SYS-1) to that of mCherry::γ-Tubulin (TEI).

217 SYS-1 and γ-Tubulin are both recruited to centrosomes at a much higher rate during mitosis than in
218 interphase (Vora and Phillips 2015; Raynaud-Messina and Merdes 2007). Because *dhc-1(ts)* limits the
219 extent of γ-Tubulin recruitment (Fig. 2B-C), evaluating SYS-1 CEI as a ratio to g-Tubulin TEI ensures that
220 decreases to the SYS-1 CEI must be disproportionately large to be numerically distinct. Consistent with
221 the published hypomorphic nature of the allele at the permissive temperature (O'rourke, Bowerman et
222 al 2007), imaging *dhc-1(ts)* embryos, shows notable decrease in the SYS-1 CEI of embryos kept at the
223 permissive temperature (Fig. 2 B-D). Following 30-45 seconds of temperature upshift, the SYS-1
224 localization hypomorphy is enhanced, severely reducing SYS-1 centrosomal enrichment (Fig. 2B-C).
225 While there was a decrease in centrosome size, presumably due to roles for dynein in centrosome
226 maturation (Priyanga, Bhakta-Guha et al 2021), we accounted for this by assessing SYS-1 CEI as a ratio to
227 the enrichment of γ-Tubulin TEI. We observed a CEI/TEI decrease corresponding to decreased
228 centrosomal SYS-1 accumulation, proportionally greater than the reduction in γ-tubulin (Fig. 2D').
229 Combined with the individual dynein subunit knockdown, the more penetrant phenotype of *dhc-1(ts)*
230 mutants indicates that SYS-1 requires the dynein microtubule motor complex to localize appropriately to
231 centrosomes. Additionally, it seems likely that redundancy of peripheral motor components or
232 incomplete knockdown is responsible for the variability within individual subunit depletions seen above
233 (Fig 1C-C').

234 **MT depolymerization experiments reveal that SYS-1 centrosomal dynamics are affected both**
235 **positively and negatively by Microtubule-Mediated trafficking**

236 To determine the extent to which microtubule-based trafficking in general is responsible for SYS-1
237 centrosomal localization, we treated gravid adults and their embryos with >100 μM Nocodazole, a
238 microtubule-destabilizing agent. This dose, while sufficient for a rapid acute response in adult animals,
239 either caused no effect on fertilized embryos because of the eggshell or prevented the production of

240 additional embryos via germline arrest (data not shown). We therefore turned to a lower dose, longer-
241 term Nocodazole treatment: 12 hours at 25μg/mL (83 μM). Maternal Nocodazole dosing allowed us to
242 obtain embryos with limited microtubule networks, but sufficient spindle development to enter mitosis
243 (Fig. 3A). Surprisingly, when treated with nocodazole, the centrosomal enrichment of the brighter P_{pie-}
244 $_{1}$::GFP::SYS-1 (GFP::SYS-1) increased after Nocodazole treatment (Fig. 3B, C).

245 The observed SYS-1 CEI increase is similar to the phenotype observed in RPT-4 depletion, which
246 decreases proteasome function (Vora and Phillips, 2015). To ensure that this change in SYS-1 localization
247 was not because of off-target effects, we compared maternal feeding to that of permeabilized embryos.
248 At 10.5 μM these embryos formed sufficient microtubule networks to enter mitosis and form spindles,
249 but these spindles were often inappropriately rotated or positioned (61% of imaged embryos, n=11/18),
250 suggesting that astral microtubules have been severely disrupted (Fig. S4A). We observed a similar CEI
251 increase in GFP::SYS-1 in these embryos (Fig. S4B). This is consistent with a model where both SYS-1
252 recruitment to centrosomes and SYS-1 proteasomal degradation are affected by disruptions to
253 microtubule mediated trafficking. Though microtubule poisoning by Nocodazole and disruption of
254 dynein function have opposite effects on SYS-1 centrosomal enrichment, either change in SYS-1
255 centrosomal enrichment may be indicative of a mis-localized regulatory process.

256 As different subsets of dynein and microtubule depletions exhibit either increased or decreased
257 SYS-1 CEI, we investigated a combination of these treatments to observe the behavior of SYS-1 upon
258 further disruption to microtubule-mediated trafficking. Moreover, while both temperature upshift for
259 *dhc-1(ts)* and Nocodazole treatments significantly affect SYS-1 centrosomal localization, neither
260 treatment appears to completely disrupt microtubule mediated trafficking. Nocodazole-treated embryos
261 still exhibit some kinetochore microtubules (Fig. 3A) but can tolerate weakly poisoned microtubules for
262 some time. Conversely, *dhc-1(ts)* embryos demonstrate such severe loss of dynein function at the

263 restrictive temperature that short-term temperature upshifts are required to establish spindles and
264 maintain viability, suggesting some portion of centrosomal trafficking during mitosis still occurs. We
265 therefore tested the combination of these treatments.

266 In contrast to embryos with GFP:SYS-1 driven by the strong early embryonic PIE-1 promoter (Fig.
267 3 B-C), embryos containing P_{sys-1}::VENUS::SYS-1, driven by the weaker endogenous SYS-1 promoter,
268 exhibit only a slight, non-significant, increase in CEI/TEI when treated with nocodazole (Fig. 3D, 1st and
269 2nd columns). However, when P_{sys-1}::VENUS::SYS-1 centrosomal enrichment is challenged by the
270 hypomorphic *dhc-1(ts)* at the permissive temperature, nocodazole treatment is sufficient to increase
271 SYS-1 centrosomal recruitment. The finding that sensitizing embryos for dynein trafficking defects is
272 required to observe a nocodazole phenotype for P_{sys-1}::VENUS::SYS-1, but not for P_{pie-1}::GFP::SYS-1
273 indicates that the difference in transgene expression uncover a differential nocodazole sensitivity in
274 centrosomal recruitment of SYS-1. However, nocodazole-mediated increase in P_{pie-1}::GFP::SYS-1
275 centrosomal enrichment is no longer observed when the nocodazole treated *dhc-1(ts)* embryos are
276 upshifted to the restrictive temperature, suggesting that the increased SYS-1 centrosomal enrichment
277 seen in nocodazole treated embryos still requires dynein trafficking.

278 These observations describe a centrosomal relationship wherein treatments limiting the
279 coverage of microtubule-mediated dynein trafficking (i.e. nocodazole treatment) increase centrosomal
280 SYS-1 because of relatively inefficient or rare trafficking events for SYS-1 negative regulators, while
281 transient severe disruptions to dynein trafficking processivity (dynein subunit RNAi depletion, *dhc-1(ts)*
282 temperature upshift, upshift + nocodazole) reveal that SYS-1 centrosomal enrichment requires continual
283 replenishment via a functional microtubule motor.

284 If the nocodazole-induced SYS-1 CEI increase described above is indeed because of a role for
285 microtubule mediated trafficking in the centrosomal enrichment of a component of the SYS-1

286 degradation pathway, we should expect proteolytic activity to be similarly mis-localized upon trafficking
287 disruption. Therefore, we decided to test the idea that proteasomal trafficking to, and enrichment at,
288 the centrosome was also perturbed in nocodazole-affected microtubule networks. We first attempted
289 to localize the proteasome. While the centrosome has been demonstrated to exhibit proteolytic activity
290 (Vora and Phillips 2015; Vora and Phillips 2016; Hames, Fry et al 2005; Peel, O'Connell et al 2012;
291 Wigley, Thomas et al 1999; Fabunmi, DeMartino et al 2000), existing immunohistochemical reagents for
292 mammalian proteasome subunits did not display any distinct localization pattern. An mCherry tag on
293 proteasome subunit RPT-1 did demonstrate a kinetochore microtubule enrichment like that of both
294 DHC-1 and SYS-1 but appeared absent from centrosomes. Inability to localize tagged RPT-1 may be due
295 to a relatively low RPT-1 copy number per proteasome, or correspondingly low proteasome number,
296 limiting its relative enrichment. Alternatively, fluorescently tagged proteins have shown evidence of
297 degradation of the tag at a site of active proteolysis, particularly if such a tag limits proteasome activity
298 (Huang, Lobel et al 2014). To circumvent this issue, we assayed for centrosomal proteasome activity
299 indirectly by functionally testing an additional centrosomal target of the RPT-4 containing proteasome,
300 the centriole duplicating kinase ZYG-1 (O'Connell, White et al 2001; Peel, O'Connell et al 2012). In
301 addition, we assayed the centrosomal role of the *C. elegans* homolog of mammalian ECM29, ECPS-1,
302 which is an adaptor protein that enhances local proteolytic activity of proteasomes via its function
303 linking the dynein motor complex and the proteasome and regulating 26S proteasome distribution
304 (Gorbea, Rechsteiner et al 2004; Gorbea, Rechsteiner et al 2010; Hsu, Cheng et al 2015; Ibañez-Vega,
305 Yuseff et al 2021).

306 Knockdown of ECM29 homolog ECPS-1 (formerly D2045.2) resulted in embryos that displayed
307 an average 33.4% increase in centrosomal P_{pie-1}::GFP::SYS-1 centrosomal enrichment, similar to both
308 Nocodazole-treated and *rpt-4(RNAi)* embryos (Fig. 4A, Fig. 3A-C). Therefore, the overall increase in SYS-1
309 CEI seen in nocodazole and *ecps-1(RNAi)* treated embryos suggests that microtubule mediated

310 trafficking enhances the removal of SYS-1 from centrosomes as well. Given the role of ECM29 in
311 proteasomal distribution via microtubule-mediated trafficking rather than directly in protein
312 degradation, these data suggest that an improperly localized proteasome in *ecps-1(RNAi)* results in
313 dysregulation of SYS-1 similar to that seen in proteasome functional knockdown (*rpt-4(RNAi))* or broader
314 depletion of microtubules (Nocodazole treatment). To determine if ECPS-1 knockdown is specific to SYS-
315 1 dysregulation, or perhaps plays a more general role in protein regulation, we assayed an additional
316 target. The ZYG-1 protein, a regulatory kinase controlling centriolar duplication, is both centrosomally
317 enriched during mitosis and negatively regulated by the RPT-4 proteasome (Peel, O'Connell et al 2012).
318 Utilizing a fluorescently tagged ZYG-1 fragment demonstrated to mirror the localization and dynamics of
319 the endogenous protein (Peters, O'Connell et al 2010), we demonstrated 20% and 27% increased
320 accumulation of ZYG-1 in both proteasome knockdown *rpt-4(RNAi)* and *ecps-1(RNAi)* treatments,
321 respectively. The similarity of phenotype between Nocodazole, ECPS-1 depletion, and RPT-4 proteasome
322 knockdown implies a microtubule-mediated trafficking link between centrosomally localized proteins
323 and their eventual degradation by the RPT-4 proteasome.

324 Since SYS-1 centrosomal recruitment depends on rapid degradation via the centrosomal
325 proteasome (Vora and Phillips 2015), we assayed the turnover rate of centrosomal SYS-1 in *ecps-1(RNAi)*
326 by FRAP. Assaying SYS-1 centrosomal turnover allowed us to assess the motility of centrosomal SYS-1.
327 Comparison of GFP::SYS-1 recovery after photobleach demonstrates that depletion of ECPS exhibits an
328 intermediate phenotype between proteasome depletion via *rpt-4(RNAi)* and negative controls (5G-G").
329 While the initial rate of *ecps-1(RNAi)* GFP::SYS-1 recovery was similar to that seen in wild type embryos,
330 the late recovery phase of *ecps-1(RNAi)* embryos showed an early SYS-1 recovery plateau, evidence of a
331 significantly reduced mobile fraction intermediate to wild type and that of proteasome depleted *rpt-*
332 *4(RNAi)* embryos (Fig. 4E,G). The recovery curve observed in *ecps-1(RNAi)* suggests that SYS-1 recovers
333 at an approximately wild type rate in *ecps-1(RNAi)* embryos but remains approximately as immobile as

334 in proteasome-depleted embryos. Therefore, ECPS-1 depleted embryos appear to degrade SYS-1
335 incompletely, as observed in the RPT-4 proteasome depletion, but with sufficient protein turnover to
336 enable wild type recruitment of newly trafficked SYS-1.

337 While both P_{pie-1}:SYS-1::GFP and P_{pie-1}::GFP::ZYG-1c exhibit an increase in their CEI because of
338 ECPS-1 depletion, their turnover rates at the centrosome are not similarly affected. The differential
339 motility between SYS-1 and ZYG-1c may be due to diverging regulatory pathways en route to the RPT-4
340 proteasome, or differential sink volumes at the mitotic centrosome. Meanwhile, ECPS-1 depleted
341 embryos may be unaffected in protein clearance per proteasome, but the delayed or partial localization
342 of the centrosomal proteasome could result in hierarchical stabilization of a spatially or temporally
343 inaccessible fraction consisting of highly expressed and continually trafficked proteins, like SYS-1.

344 **Dynein Trafficking is Required for Restriction of Wnt-Signaled Cell Fates**

345 Having established a two-fold role for SYS-1 regulation in microtubule-mediated trafficking, we
346 investigated the role microtubule trafficking played in regulating SYS-1 dependent cell fate decisions.
347 Since the SYS-1 centrosomal localization pattern has been seen across all examined SYS-1-expressing
348 tissues (Phillips, Kimble et al 2007; Huang, Lin et al 2007; Baldwin and Phillips 2018; Lam and Phillips
349 2017), we investigated cell fate changes in embryonic and larval tissues across one embryonic and two
350 larval SYS-1 dependent cell fate decisions. These included the transcriptional reporter of the WβA target
351 gene, *end-1,* in the establishment of SYS-1 dependent endoderm, and an anatomical marker for larval
352 specification of the stem cell-like cells of the hypodermal seam and the germline stem cell niche. First, to
353 directly assay the effect of centrosomal dysregulation of transcriptional activator SYS-1, we investigated
354 the nuclear enrichment of GFP::SYS-1 after the Wnt-regulated EMS division (Bei, Mello et al 2002). In
355 the EMS division, SYS-1 is enriched in the posterior E nucleus, but not that of the anterior MS (Fig. 5A-B).
356 Analyzing nuclear enrichment of GFP-tagged SYS-1, we were able to observe increased nuclear GFP

357 signal in both the E and MS daughters in analyzed trafficking mutants (Fig. 5C). Interestingly, daughters
358 affected by both *ecps-1(RNAi)* and *dlc-1(RNAi)* exhibit significant enhancement of nuclear enrichment in
359 each of the two daughter cells (Fig 5C), suggesting that these treatments act negatively on SYS-1, despite
360 opposing effect on SYS-1 centrosomal enrichment. Following loss of negative centrosomal regulation,
361 these data suggest that daughter cell SYS-1 inheritance is increasing and thus affecting the bias of the
362 EMS asymmetric division, increasing the likelihood of unsignaled daughter cells adopting the signaled
363 endoderm cell fate.

364 Having established an increase in nuclear GFP::SYS-1 in dynein subunit depletion, even in cells
365 not signaled to maintain activating SYS-1, we turned to the effect of SYS-1 expression on target gene
366 activation. Specifically, we used the endogenous promoter of WβA target gene *end-1* to drive GFP-
367 tagged Histone 2B in order to evaluate the activity of SYS-1 immediate downstream targets as the
368 signaled E cell established the endoderm tissue expansion from 2 to 4 to 8 cells (E+1, 2, or 3 divisions,
369 respectively). Normally, this strain exhibits additional expression of the *end-1* promoter in <10% of
370 embryos, a frequency which decreases further when SYS-1 is depleted via RNAi (Fig. 5D). In embryos
371 depleted of either dynein subunits or RSA-2 by RNAi, however, we observed a different pattern. In these
372 embryos, misregulation via dynein depletion appeared to increasingly overwhelm SYS-1 negative
373 regulation in successive divisions, such that each generation after SYS-1 dependent specification
374 increasingly expresses the *end-1* promoter driven endodermal reporter outside of the EMS lineage (Fig.
375 5D). For instance, in *dhc-1(RNAi)* we observe only 3% of embryos mis-expressing one cell division after
376 the specification of the E cell type (E+1), which increases to 25% by the next division (E+2), and over 83%
377 three divisions after specification (E+3).

378 We also investigated larval ACDs to determine the effect that extra transcriptionally active SYS-1
379 has on organismal development. We examined the seam cells (SCs) and distal tip cells (DTCs) because of

380 their sensitivity to SYS-1 dependent gene activation (Baldwin, Phillips et al 2016; Baldwin and Phillips
381 2018; Lam and Phillips 2017; Mila, Putzke et al 2015). In wild-type animals, DTC lineages undergo
382 asymmetric cell division during L1 to give rise to two DTCs, while *sys-1* mutants and animals
383 overexpressing SYS-1 show loss or gain of DTCs, respectively, due to symmetric cell division (Fig 6A)
384 (Miskowski, Kimble et al 2001; Siegfried, Kimble et al 2004; Kidd, Kimble et al 2005; Chesney, Kimble et
385 al 2009). To further sensitize these cells for changes in SYS-1 dependent cell fate changes, we examined
386 strains containing additional, transgenic SYS-1 driven by the heat shock promoter. In animals that are
387 not subjected to heat shock, dynein depletion only rarely induced development of more than the
388 endogenous 2 distal tip or 16 seam cells (Fig. 6B, 7B). In heat shocked animals, excess SYS-1 protein can
389 overwhelm canonical SYS-1 regulation to develop as many as 6 DTCs (Fig. 6D). While heat shock-induced
390 overexpression is sufficient to cause a notable shift towards the signaled cell fate, dynein subunit
391 depletion was able to significantly enhance the effect of heat shock (Fig. 6C). Depletion of DHC-1 or
392 ECPS-1 at the time of the somatic gonadal precursor division was sufficient to induce rare but wild-type-
393 unobserved additional DTCs (0.3% of animals for these 2 treatments, N= 394, 363, respectively). Adding
394 heat shock-overexpressed SYS-1 enhanced the penetrance of ectopic DTCs, with DHC-1 and ECPS-1
395 depletion resulting in populations where 11.9% and 6.8% of animals, respectively, develop more than 2
396 DTCs. Depletion of RSA-2, uncoupling SYS-1 from centrosomes, and depletion of a dynein light chain,
397 DYLT-1, further enhanced these misspecifications, increasing the proportion of the population with
398 ectopic DTCs from 26.6% in wild type to 33.6% or 51% after RNAi depletion, respectively (Fig. 6D).

399 The SC lineage also undergoes several WβA-dependent ACDs throughout larval development
400 (Fig 7A). Similarly, in the SC tissue, depletion of dynein light chains alone is sufficient to increase the
401 frequency of ectopic SCs from 3.3% of larvae with ectopic SCs in control RNAi conditions to 11.7% or
402 10% of animals as seen in DYLT-1 and DLC-1 depletions, respectively (Fig. 7B). These misspecifications
403 are further exacerbated by SYS-1 overexpression, wherein more than 60% of the *dylt-1(RNAi)* larvae

404 have greater than wild type seam cell numbers, developing as many as 21 SCs, (Fig. 7C). These
405 observations collectively support SYS-1 centrosomal enrichment by dynein as a mechanism to reinforce
406 SYS-1 function in specifying SYS-1-dependent cell fate decisions. Therefore, compromising the
407 centrosomal SYS-1 regulatory system by dynein depletion is rarely sufficient to induce misspecifications
408 in otherwise wildtype animals, but notably enhances the effects of ectopic SYS-1 accumulation.
409 Therefore, dynein-dependent centrosomal regulation of transcriptional coactivator SYS-1 increases the
410 robustness of WβA-regulated cell fate decisions after ACD.

411 **Discussion**

412 Precise control of cell fate determinants is critical for normal development and homeostasis,
413 particularly in the rapidly dividing cells of the early embryo. Regulation of these factors includes the
414 distribution and inheritance of these determinants by daughter cells. Here we demonstrate that
415 centrosomal negative regulation of *C. elegans* β-catenin SYS-1 is enhanced during asymmetric division
416 by trafficking to centrosomes by the microtubule motor dynein. Depletion of individual subunits of the
417 dynein motor and associated proteins is sufficient to reduce the levels of centrosomal SYS-1, and
418 temporally specific ablation of dynein function by *dhc-1(ts)* was sufficient to remove observable SYS-1
419 nearly completely and disproportionately from centrosomes. However, some methods of disrupting
420 dynein/microtubule trafficking result in an unexpected increase in centrosomal accumulation of SYS-1
421 protein. These increases, caused by microtubule disruption via Nocodazole and depletion of SYS-1
422 negative regulator adapter ECPS-1 phenocopy centrosomal enrichment seen in disruption of
423 proteasome activity, and maintain a SYS-1 immobile fraction like that seen in *rpt-4(RNAi)* depletion. We
424 therefore propose a model wherein both SYS-1 and regulatory components of the ubiquitin-proteasome
425 system, are dependent on microtubule-mediated trafficking to centrosomes by the dynein complex in
426 order to appropriately reinforce SYS-1 asymmetric regulation across daughter cells (Fig. 8).

427 In this model, SYS-1 enriches at centrosomes and is degraded or marked for degradation before
428 leaving the centrosome. Rather than a static centrosomal enrichment, this model entails continual
429 trafficking by microtubule motors to maintain an observable centrosomal pool of SYS-1. The observable
430 CEI therefore measures a steady state of centrosomal enrichment at centrosomes, wherein SYS-1 is
431 localized to centrosomes more rapidly than it is marked and cleared. SYS-1 therefore becomes visibly
432 enriched at centrosomes compared to cytoplasmic levels. This model predicts that even subtle
433 disruptions to microtubule mediated trafficking could limit the ability of cells to maintain wild type SYS-1
434 centrosomal enrichment, assuming the SYS-1 clearance rate remains unchanged.

435 Interestingly, the *rsa-2(RNAi)* enhancement of kinetochore localization of SYS-1 in this model is
436 consistent with 'traffic jams' observed in microtubule mediated trafficking (Leduc, Howard et al 2012). In
437 these cases, crowding motors by increasing the local concentration of motor proteins, introducing
438 microtubule-binding obstacles, or, importantly for our model, preventing motor dissociation limits the
439 activity of motor proteins (Nam and Epureanu, 2017; Ferro, Yildiz et al 2019). Evidence of traffic jams in
440 vivo have been shown in neuronal microtubule transport, as neuronal kinesin and its cargo
441 synaptotagmin accumulate when trafficking is disrupted by hypomorphic kinesin alleles. The disrupted
442 motor complexes then accumulate upstream of the trafficking impediment, in an accumulation of both
443 motor and cargo (Hurd and Saxton 1996).

444 The kinetochore localization of SYS-1 is consistent with a traffic jam model, thus making SYS-1 trafficking
445 by microtubule motors a more attractive model. Decreasing centrosomal SYS-1 localization by *rsa-*
446 *2(RNAi)* increases SYS-1 protein in resulting daughter cells (Vora and Phillips 2015). A severely limited
447 centrosomal recruitment of SYS-1 in *rsa-2(RNAi)* may also suggest problematic SYS-1/motor protein
448 unloading upon reaching the MTOC centrosome. Similarly, P_{pie-1}::GFP::SYS-1, which appears
449 overexpressed compared to P_{sys-1}::VENUS::SYS-1, may exacerbate SYS-1 traffic jams by increasing the
450 cytoplasmic SYS-1 pool. Indeed, the combination of P_{pie-1}::GFP::SYS-1 and *rsa-2(RNAi)* results in a further

451 increase in the incidence of SYS-1 localization to kinetochore microtubules, suggesting increased SYS-1
452 levels coupled with decreased centrosomal capturing may reveal an otherwise transient pool of SYS-1 en
453 route to the MTOC centrosome. Inefficient SYS-1 capture in *rsa-2(RNAi)* embryos likely further crowds
454 SYS-1-containing microtubule motor complexes into 'traffic jams' because, in embryos lacking a
455 mechanism to anchor SYS-1 to the centrosome, SYS-1 is trafficked toward centrosomes more quickly
456 than it is captured there and processed. This shift results in an observable SYS-1 accumulation at regions
457 of high microtubule occupancy, such as kinetochore microtubules and the cell cortex, both of which are
458 increased after RSA-2 depletion.

459 Conversely, centrosomal protein processing by either post-translational modifications or
460 degradation via the proteasome likely requires the trafficking of fewer, yet reusable enzymes. The
461 disparity between substrate vs enzyme trafficking requirements would suggest that clearance of
462 centrosomal substrates is less vulnerable to mild or short-term disruptions to trafficking than the
463 maintenance of a centrosomal substrate pool. Upon long-term or severe disruptions to microtubule
464 trafficking, a trafficking requirement for clearance mechanisms becomes apparent. Our model predicts
465 that disruption of either SYS-1 localization (inefficient trafficking to the site of regulation) or disrupting
466 the localization of a member of the Ubiquitin-Proteasome System (UPS) (where SYS-1 is trafficked and
467 accumulates, but centrosomal regulation/degradation is ineffective) both result in increased SYS-1
468 dependent gene activation and differentiation in daughter cells, consistent with excessive inheritance.
469 While this system of centrosomal localization and clearance of SYS-1 does not appear necessary for most
470 WβA differentiation events, disruptions to SYS-1 trafficking or processing limit the system's ability to
471 tolerate perturbations. That is, SYS-1 centrosomal localization generates robustness in SYS-1 dependent
472 cell fate decisions (Fig. -7) due to parallel trafficking mechanisms; disrupting either trafficking
473 mechanism results in excessive SYS-1 dependent activity in daughter cells of mothers with either
474 increased or decreased SYS-1 CEI.

475 Why does no single dynein disruption treatment fully recapitulate the *rsa-2(RNAi)* phenotype?
476 While we see individuals within several dynein knockdown treatments with nearly *rsa-2(RNAi)*-like SYS-1
477 centrosomal uncoupling, these populations also include embryos with roughly wild type centrosomal
478 SYS-1 enrichment. However, given the severely deleterious nature of dynein subunit loss-of-functions
479 (Sönnichsen, Neumann et al 2005) and the variability of feeding RNAi knockdowns as compared to null
480 mutant strains (Tavernarakis, Driscoll et al 2000), it seems likely that our significant decreases in SYS-1
481 centrosomal recruitment represent a phenotypically incomplete knockdown. Surviving embryos then
482 only exhibit hypomorphic dynein function, insufficient to induce catastrophic defects in spindle
483 assembly but sufficient to affect SYS-1 centrosomal enrichment. However, it is also possible that there is
484 partial redundancy between the SYS-1 relevant functions of the dynein motor. Introducing *dhc-1(ts)*
485 overcomes either incomplete knockdown or redundancy since a thorough dynein disruption is able to
486 robustly uncouple centrosomal SYS-1.

487 Why, then, do we observe an increase in centrosomal SYS-1 steady state upon either long term
488 lower dose nocodazole-mediated knockdowns of trafficking or by RNAi depletion of trafficking subunit
489 ECPS-1? In response to these data (Fig. 3), we propose the additional trafficking of a SYS-1 negative
490 regulatory component to this model. Disrupting the trafficking of centrosomal SYS-1 negative regulators
491 should result in a previously unseen increase in centrosomal SYS-1 steady state while maintaining a
492 similar effect on downstream gene expression and cell fate decisions, as seen above (Fig. 3-7). However,
493 the difference in SYS-1 enrichment between most dynein depletions and that of ECPS-1 or nocodazole
494 treatment suggests a differential efficiency in trafficking or centrosomal capture rate between SYS-1 and
495 its negative regulators, such as the proteasome. Most disruptions to the dynein motor that reduce SYS-1
496 centrosomal accumulation, mediated by maternally fed RNAi, are consistent but likely incomplete
497 because of their requirement for oogenesis and early embryonic viability. Relatively mild dynein
498 knockdowns resulting in viable embryos, therefore, are likely able to form dynein complexes, but at a far

499 reduced rate. These dynein-limited embryos should therefore decrease the rate of continual SYS-1
500 trafficking while not preventing the centrosomal localization of an occasional regulatory components,
501 perhaps of the Ubiquitin-Proteasome System (UPS). The reusable tagging or proteolytic machinery is
502 likely sufficient to enzymatically process SYS-1 that still localizes to the centrosome, but the rate of
503 incoming SYS-1 is significantly reduced. Similarly, depletion of dynein function by *dhc-1(ts)* effectively
504 depletes all dynein function but can only do so for brief portions of mitosis without inducing mitotic
505 spindle collapse.

506 While dynein depletions limit the volume of trafficking by limiting the number of properly
507 constructed dynein motors, they do not limit the ability of an individual, functional dynein motor to
508 traffic. The experimental conditions that increase the steady state of centrosomal SYS-1, Nocodazole
509 and *ecps-1(RNAi)*, instead limit the scope of dynein cargo trafficking. ECPS-1, putative adapter between
510 dynein and the proteasome, increases the steady state of both SYS-1 and additional centrosomal
511 proteasome target ZYG-1. Increased enrichment of both proteins is consistent with the conserved role
512 of ECM29 for ECPS-1, and results in embryos that are not inhibited for overall dynein function but
513 limited in their ability to traffic proteasome. Nocodazole treatment similarly does not directly affect the
514 processivity of dynein complexes that form on the comparatively limited microtubule network.
515 However, it does severely affect the reach of the microtubule network itself (Fig. 3A). Our data therefore
516 suggests that the proteasome requires less continual reinforcement by microtubule-mediated trafficking
517 but does require more extensive microtubule formation than is allowed in our Nocodazole-treated
518 embryos.

519 A role for trafficking in both SYS-1 and its regulatory components, then, suggests a differentially
520 maintained steady state interaction for the proteasome and centrosomal SYS-1. While SYS-1 is rapidly
521 and continuously trafficked, it is similarly rapidly processed by centrosomal proteasome. That is, the
522 apparently rapid processing of centrosomal SYS-1 also requires rapid dynein-mediated flux to maintain

523 its centrosomal steady state. Any disruption to dynein processivity will therefore allow slower SYS-1
524 centrosomal enrichment to be overcome by its centrosomal processing, reducing the SYS-1 CEI by
525 slowing the transfer of SYS-1 from cytoplasm to centrosome for degradation. By comparison, the
526 proteasome or ubiquitin ligases endure at the centrosome, continually processing centrosomal targets.
527 Our proposed model therefore predicts that short term or partial disruptions to the dynein motor (Fig.
528 8, red inset) allow for the eventual establishment of a centrosomal proteolysis pathway, which may
529 affect both SYS-1 and proteasome localization, but nevertheless result in decreasing steady state levels
530 of centrosomal SYS-1 (and presumably other proteasome targets that require active trafficking) as
531 occasional proteasome centrosomal localization overcomes the impaired localization of SYS-1.
532 Conversely, long term systemic disruptions to microtubule-mediated motors like that seen in
533 Nocodazole treatment may still capture SYS-1 in their comparatively limited microtubule network, while
534 being disproportionately deprived of the larger proteasome complex (Fig. 8, blue inset).

535 Our model that both SYS-1 and its regulators are trafficked was supported but the identification
536 of a trafficking component that affects one but not both arms of our trafficking model. Most of our
537 perturbations, generally affecting components of the dynein machinery, may exert their effects by
538 either detaching SYS-1 from the motor or by sabotaging all function of the motor complex. However, the
539 specificity of our two transport mechanisms was exhibited by one dynein-protein interaction, via
540 depletion of ECPS-1/the putative ECM29 subunit of the motor. Unlike the other subunits presenting
541 strong SYS-1 phenotypes, ECM29 has not yet been implicated in dynein function beyond its adaptor role
542 but has notable effects on proteasome localization and response to stress (Gorbea, Rechsteiner et al
543 2010; Haratake, Chiba et al 2016). Because *ecps-1(RNAi)* phenocopies the centrosomal GFP::SYS-1
544 accumulation seen in proteasome knockdown via *rpt-4(RNAi)* as well as microtubule network disruption
545 via Nocodazole treatment, we propose that these observations support a role for proteasomal
546 localization as well as function for proper centrosomal clearance of SYS-1 (Fig. 8).

547 While this model and our experiments to test it have been largely centered on SYS-1/β-catenin,
548 many developmental and temporally regulated proteins are known to pass through the centrosome
549 (Vora and Phillips 2016; Brown, Welch et al 1994; Johnston, Kopito et al 1998; Huang and Raff 1999;
550 Reck-Peterson, Carter et al 2018), as the centrosomal proteasome is far from SYS-1-specific. It is not
551 unreasonable, then, to presume that other proteins may benefit from dynein trafficking to something as
552 short-lived and yet influential to daughter cell inheritance as the mitotic centrosome. Particularly early
553 in eukaryotic development, subtle changes in the inheritance of cell fate determinants like SYS-1 can
554 have a profound effect on the ability of an organism to respond to environmental insults. For example,
555 the asymmetric nuclear localization of SYS-1 indicative of differential cell fate has been shown to arise
556 early, less than 70 seconds after the establishing division (Baldwin and Phillips 2014; Vora and Phillips
557 2015). We therefore propose that an active dynein mediated trafficking, at least for cell fate
558 determinants like SYS-1, could provide a universal buffering against excessive inheritance and
559 consequentially rare but deleterious cell fate changes.

560 **Materials and Methods**

561 **Strains**

562 Strains were maintained on Op50-inoculated NGM plates at 15° (BTP51, BTP220) or 25° C
563 (TX964, BTP51, LP563, TX691) using typical *C. elegans* methods. These strains contained the following
564 transgenes and alleles: **N2** (wild type); **TX964** (unc-119(ed3) III; him-3(e1147) IV; teis98 [Ppie-
565 1::GFP::SYS-1]); **BTP51** (unc-119(ed3) III; tjIs71 [pie-1 promoter::mCherry::H2B, pie-1 promoter::2x
566 mCherry::tbg-1, unc-119(+)]; qIs95 III) ; **BTP220** (unc-119(ed3) III; tjIs71 [pie-1 promoter::mCherry::H2B,
567 pie-1 promoter::2x mCherry::tbg-1, unc-119(+)]; qIs95 III; dhc-1(or195) I.) ; **TX691** (unc-119(ed3) III;
568 teIs46 [pRL1417; end-1p::GFP::H2B + unc-119(+)]) ; **OC341 (**unc-119(ed3) III; bsIs8[pMS5.1:unc -119(+)
569 pie -1- gfp-zyg-1C-terminus]); **BTP93** (*wIs78[SCMp::GFP + ajm-1p::GFP + F58E10* (cosmid) *+ unc-119(+*)]

570 *IV; uiwEx22*[*pHS::sys-1*]); **BTP97** (*qIs56[lag-2p::GFP + unc-119(+)] V;uiwIs3[pHS::sys-1*]); **AZ235** (*unc-*

571 *119(ed3) III; ruIs48[Ppie-1::gfp::tbb-1*]; **TH107 (**P_{pie-1}::RSA-2:: GFP)

572 **RNAi**

573 To perform RNAi knockdown of target genes, we used HT115 bacteria containing the pL4440

574 plasmid with a T7-flanked target gene insert. Most of these were obtained from a library supplied by

575 Ahringer (Kamath and Ahringer 2003). Those which were otherwise obtained (dlc-1) used target gene-

576 flanking primers with *C. elegans* cDNA to generate a new insert. These bacteria were used to seed IPTG-

577 containing, inducing plates as described previously. Worms were generally plated to RNAi after Sodium

578 Hypochlorite Synchronization as L1's. More deleterious knockdowns (*dlc-1, dhc-1)* were washed from

579 OP50 plates at 24 hours before imaging (L3/L4) or 12 hours before imaging (late L4/early adult)

580 (Timmons 2006; Bekas and Phillips 2020). DLC-1 was derived using RT primers and digested with Xho I

581 and HIND III SEQUENCING 7/31

582 **Compound Microscopy, CEI, and Image Processing**

583 To obtain samples, mothers were anesthetized with 250 μM levamisole and dissected *via* a

584 clean surgical blade. Embryos were then transferred to a 2% agarose pad and imaged on a Zeiss Axio

585 Imager.D2. All exposure times were kept constant. Centrosomal measurements were collected from the

586 mitotic P1 cell of the early embryo during anaphase, at approximately similar inter-polar distance (Fig.

587 S5). Images were exported as uncompressed TIF's, and fluorescence intensity was determined by

588 measuring the mean fluorescence of centrosomal puncta in ImageJ. The mean intensity of the remaining

589 embryonic cytoplasm was subtracted from the centrosomal mean to produce the CEI measurement, and

590 identical measurements on 2x mCherry::tbg-1 were used for TEI. END-1 family nuclei were assayed via

591 the TX691 strain. GFP-tagged Histone intensity was measured relative to the cytoplasmic

592 autofluorescence.

593 **Temperature Sensitive Allele Imaging**

594 BTP51 and BTP220 were maintained together at 15°C and were imaged as above. Ambient
595 temperature in the microscope room was decreased to ~18°C for 'permissive' imaging and upshifted to
596 'restrictive' 26°C by moving slides to a Pecon Tempcontroller 2000-2 heated stage. Embryos were
597 imaged at the two temperatures sequentially, with approx. 45 seconds between upshift and image, or
598 were imaged as populations at either the permissive or restrictive temperature.

599 **Nocodazole Treatment**

600 In order to treat embryos before formation of the drug-impermeable eggshell, we exposed late
601 L4's to a low dose (approx. 83 μM, 25 μg/mL) nocodazole dissolved in 2% DMSO for 16 hours. Embryos
602 were then concentrated by one minute centrifugation at 1000xG and imaged as described above.
603 Permeabilization of embryos was performed as described in Carvalho, Oegema et al 2011. Imaging was
604 done as described above, but included 4% sucrose and 0.1M NaCl to the 2% agar pads to bolster embryo
605 stability (Greenan, Hyman et al 2010; Gönczy, Schnabel et al 1999).

606 **Confocal Microscopy and Fluorescence Recovery After Photobleach**

607 Confocal microscopy was performed via a Leica SP8 HyD detector system. The objective used
608 was a 63x HC PL APO CS2 objective with N.A. = 1.4, utilizing type F immersion oil. Each image analyzed
609 consisted of the sum of 35 z-images across the embryo, each slice approximately 0.35 μM thick. FRAP
610 was performed on the same system. Each embryo was imaged twice before bleaching, beginning as
611 soon as possible after NEBD. The ROI, an approximately 5μm square, was then bleached at an
612 intermediate focal plane with 100% laser power for 100 iterations. Images were taken as above, once
613 every 7 seconds. Fluorescence intensity was measured on summed slice Z-projections in FIJI via the
614 mean fluorescence intensity of ROIs drawn around relevant locales – either centrosome or the entire

615 dividing cell. Recovery was assayed by subtracting the ROI post-bleach intensity from each
616 measurement and evaluating it as a percentage of the pre-bleached centrosomal intensity.

617 **Heat Shock-Induced SYS-1 Overexpression**

618 BTP93 and BTP97 worms were exposed to brief 33°C heat shocks at relevant developmental
619 timepoints to drive SYS-1 overexpression concurrently with signaled cell fate specification. For DTCs,
620 BTP97 was subjected to 1-hour heat shock, 30-minutes recovery, and 30-minutes additional heat shock
621 beginning 11.5 hours after plating. For SCs, BTP93 was subjected to 2-hour heat shock, 30-minute
622 recovery, and additional 1-hour heat shock beginning 26 hours after plating. Both tissue types were
623 assayed 50 hours after plating.

624 **Acknowledgements**

625 We thank Kimberly Bekas and Amy Clemons for helpful comments on the manuscript. Strains
626 were provided by the Caenorhabditis Genetics Center, which is funded by the National Institutes of
627 Health (NIH) Office of Research Infrastructure Programs [P40 OD01440], or gifts from the laboratory of
628 Tony Hyman (TH107) and Dr. Kevin F. O'Connell at the NIDDK (OC341). This work was supported by NIH
629 award NIH GM114007 (B.T.P.).

630

631

632

633

634

635

636 **References**

637 Amsterdam, A., F. Pitzer and W. Baumeister (1993). "Changes in intracellular localization of proteasomes
638 in immortalized ovarian granulosa cells during mitosis associated with a role in cell cycle control." Proc
639 Natl Acad Sci U S A **90**(1): 99-103.

640 Baldin, V., M. Militello, Y. Thomas, C. Doucet, W. Fic, S. Boireau, I. Jariel-Encontre, M. Piechaczyk, E.
641 Bertrand, J. Tazi and O. Coux (2008). "A novel role for PA28gamma-proteasome in nuclear speckle
642 organization and SR protein trafficking." Mol Biol Cell **19**(4): 1706-1716.

643 Baldwin, A. T., A. M. Clemons and B. T. Phillips (2016). "Unique and redundant beta-catenin regulatory
644 roles of two Dishevelled paralogs during C. elegans asymmetric cell division." J Cell Sci **129**(5): 983-993.

645 Baldwin, A. T. and B. T. Phillips (2014). "The tumor suppressor APC differentially regulates multiple beta-
646 catenins through the function of axin and CKIalpha during C. elegans asymmetric stem cell divisions." J
647 Cell Sci **127**(Pt 12): 2771-2781.

648 Baldwin, A. T. and B. T. Phillips (2018). Chapter 3 - Cell Polarity and Asymmetric Cell Division by the Wnt
649 Morphogen. Cell Polarity in Development and Disease. P. Michael Conn. Boston, Academic Press**:** 61-
650 102.

651 Bei, Y., J. Hogan, L. A. Berkowitz, M. Soto, C. E. Rocheleau, K. M. Pang, J. Collins and C. C. Mello (2002).
652 "SRC-1 and Wnt signaling act together to specify endoderm and to control cleavage orientation in early
653 C. elegans embryos." Dev Cell **3**(1): 113-125.

654 Bekas, K. N. and B. T. Phillips (2020). "Generating reliable hypomorphic phenocopies by RNAi using long
655 dsRNA as diluent." MicroPubl Biol **2020**.

656 Ben-Yaakov, K., S. Y. Dagan, Y. Segal-Ruder, O. Shalem, D. Vuppalanchi, D. E. Willis, D. Yudin, I. Rishal, F.
657 Rother, M. Bader, A. Blesch, Y. Pilpel, J. L. Twiss and M. Fainzilber (2012). "Axonal transcription factors
658 signal retrogradely in lesioned peripheral nerve." EMBO J **31**(6): 1350-1363.

659 Bullock, S. L. and D. Ish-Horowicz (2001). "Conserved signals and machinery for RNA transport in
660 Drosophila oogenesis and embryogenesis." Nature **414**(6864): 611-616.
661 Carminati, J. L. and T. Stearns (1997). "Microtubules orient the mitotic spindle in yeast through dynein-
662 dependent interactions with the cell cortex." J Cell Biol **138**(3): 629-641.
663 Chesney, M. A., N. Lam, D. E. Morgan, B. T. Phillips and J. Kimble (2009). "C. elegans HLH-
664 2/E/Daughterless controls key regulatory cells during gonadogenesis." Dev Biol **331**(1): 14-25.
665 del Castillo, U., M. Winding, W. Lu and V. I. Gelfand (2015). "Interplay between kinesin-1 and cortical
666 dynein during axonal outgrowth and microtubule organization in Drosophila neurons." Elife **4**: e10140.
667 Deshimaru, M., M. Kinoshita-Kawada, K. Kubota, T. Watanabe, Y. Tanaka, S. Hirano, F. Ishidate, M.
668 Hiramoto, M. Ishikawa, Y. Uehara, H. Okano, S. Hirose, S. Fujioka, K. Iwasaki, J. Yuasa-Kawada, T.
669 Mishima and Y. Tsuboi (2021). "DCTN1 Binds to TDP-43 and Regulates TDP-43 Aggregation." Int J Mol Sci
670 **22**(8).
671 Fabunmi, R., W. Wigley, P. Thomas and G. DeMartino (2000). "Activity and Regulation of the
672 Centrosome-associated Proteasome." Journal of Biological Chemistry **275**: 409-413.
673 Fan, J., Q. Zhang, H. Tochio, M. Li and M. Zhang (2001). "Structural basis of diverse sequence-dependent
674 target recognition by the 8 kDa dynein light chain." J Mol Biol **306**(1): 97-108.
675 Ferenz, N. P., A. Gable and P. Wadsworth (2010). "Mitotic functions of kinesin-5." Seminars in cell &
676 developmental biology **21**(3): 255-259.
677 Fuchs, E. and T. Chen (2013). "A matter of life and death: self-renewal in stem cells." EMBO Rep **14**(1):
678 39-48.
679 Gao, F. J., L. Shi, T. Hines, S. Hebbar, K. L. Neufeld and D. S. Smith (2017). "Insulin signaling regulates a
680 functional interaction between adenomatous polyposis coli and cytoplasmic dynein." Mol Biol Cell **28**(5):
681 587-599.

682 Geyer, F. C., M. Lacroix-Triki, K. Savage, M. Arnedos, M. B. Lambros, A. MacKay, R. Natrajan and J. S.
683 Reis-Filho (2011). "beta-Catenin pathway activation in breast cancer is associated with triple-negative
684 phenotype but not with CTNNB1 mutation." Mod Pathol **24**(2): 209-231.
685 Gómez-López, S., R. G. Lerner and C. Petritsch (2014). "Asymmetric cell division of stem and progenitor
686 cells during homeostasis and cancer." Cell Mol Life Sci **71**(4): 575-597.
687 Gönczy, P., H. Schnabel, T. Kaletta, A. D. Amores, T. Hyman and R. Schnabel (1999). "Dissection of Cell
688 Division Processes in the One Cell Stage Caenorhabditis elegans Embryo by Mutational Analysis." Journal
689 of Cell Biology **144**(5): 927-946.
690 Gorbea, C., G. M. Goellner, K. Teter, R. K. Holmes and M. Rechsteiner (2004). "Characterization of
691 mammalian Ecm29, a 26 S proteasome-associated protein that localizes to the nucleus and membrane
692 vesicles." J Biol Chem **279**(52): 54849-54861.
693 Gorbea, C., G. Pratt, V. Ustrell, R. Bell, S. Sahasrabudhe, R. E. Hughes and M. Rechsteiner (2010). "A
694 protein interaction network for Ecm29 links the 26 S proteasome to molecular motors and endosomal
695 components." J Biol Chem **285**(41): 31616-31633.
696 Greenan, G., C. P. Brangwynne, S. Jaensch, J. Gharakhani, F. Jülicher *et al.*, 2010 Centrosome size sets
697 mitotic spindle length in Caenorhabditis elegans embryos. Curr Biol 20**:** 353-358.
698 Hames, R. S., R. E. Crookes, K. R. Straatman, A. Merdes, M. J. Hayes, A. J. Faragher and A. M. Fry (2005).
699 "Dynamic recruitment of Nek2 kinase to the centrosome involves microtubules, PCM-1, and localized
700 proteasomal degradation." Mol Biol Cell **16**(4): 1711-1724.
701 Hamill, D. R., A. F. Severson, J. C. Carter and B. Bowerman (2002). "Centrosome maturation and mitotic
702 spindle assembly in C. elegans require SPD-5, a protein with multiple coiled-coil domains." Dev Cell **3**(5):
703 673-684.

704 Hanz, S., E. Perlson, D. Willis, J. Q. Zheng, R. Massarwa, J. J. Huerta, M. Koltzenburg, M. Kohler, J. van-
705 Minnen, J. L. Twiss and M. Fainzilber (2003). "Axoplasmic importins enable retrograde injury signaling in
706 lesioned nerve." Neuron **40**(6): 1095-1104.
707 Harada, A., Y. Takei, Y. Kanai, Y. Tanaka, S. Nonaka and N. Hirokawa (1998). "Golgi vesiculation and
708 lysosome dispersion in cells lacking cytoplasmic dynein." J Cell Biol **141**(1): 51-59.
709 Haratake, K., A. Sato, F. Tsuruta and T. Chiba (2016). "KIAA0368-deficiency affects disassembly of 26S
710 proteasome under oxidative stress condition." J Biochem **159**(6): 609-618.
711 He, T. C., A. B. Sparks, C. Rago, H. Hermeking, L. Zawel, L. T. da Costa, P. J. Morin, B. Vogelstein and K. W.
712 Kinzler (1998). "Identification of c-MYC as a target of the APC pathway." Science **281**(5382): 1509-1512.
713 Horgan, C. P., S. R. Hanscom, R. S. Jolly, C. E. Futter and M. W. McCaffrey (2010). "Rab11-FIP3 links the
714 Rab11 GTPase and cytoplasmic dynein to mediate transport to the endosomal-recycling compartment."
715 J Cell Sci **123**(Pt 2): 181-191.
716 Hsu, M. T., C. L. Guo, A. Y. Liou, T. Y. Chang, M. C. Ng, B. I. Florea, H. S. Overkleeft, Y. L. Wu, J. C. Liao and
717 P. L. Cheng (2015). "Stage-Dependent Axon Transport of Proteasomes Contributes to Axon
718 Development." Dev Cell **35**(4): 418-431.
719 Huang, L., D. Pike, D. E. Sleat, V. Nanda and P. Lobel (2014). "Potential pitfalls and solutions for use of
720 fluorescent fusion proteins to study the lysosome." PLoS One **9**(2): e88893.
721 Huang, S., P. Shetty, S. M. Robertson and R. Lin (2007). "Binary cell fate specification during C. elegans
722 embryogenesis driven by reiterated reciprocal asymmetry of TCF POP-1 and its coactivator beta-catenin
723 SYS-1." Development **134**(14): 2685-2695.
724 Hutagalung, A. H. and P. J. Novick (2011). "Role of Rab GTPases in membrane traffic and cell physiology."
725 Physiol Rev **91**(1): 119-149.

726 Ibañez-Vega, J., F. Del Valle, J. J. Sáez, F. Guzman, J. Diaz, A. Soza and M. I. Yuseff (2021). "Ecm29-
727 Dependent Proteasome Localization Regulates Cytoskeleton Remodeling at the Immune Synapse." Front
728 Cell Dev Biol **9**: 650817.
729 Jha, R. and T. Surrey (2015). "Regulation of processive motion and microtubule localization of
730 cytoplasmic dynein." Biochem Soc Trans **43**(1): 48-57.
731 Juanes, M. A. (2020). "Cytoskeletal Control and Wnt Signaling-APC's Dual Contributions in Stem Cell
732 Division and Colorectal Cancer." Cancers (Basel) **12**(12).
733 Kamath, R. S., A. G. Fraser, Y. Dong, G. Poulin, R. Durbin, M. Gotta, A. Kanapin, N. Le Bot, S. Moreno, M.
734 Sohrmann, D. P. Welchman, P. Zipperlen and J. Ahringer (2003). "Systematic functional analysis of the
735 Caenorhabditis elegans genome using RNAi." Nature **421**(6920): 231-237.
736 Kawaguchi, Y., J. J. Kovacs, A. McLaurin, J. M. Vance, A. Ito and T. P. Yao (2003). "The deacetylase HDAC6
737 regulates aggresome formation and cell viability in response to misfolded protein stress." Cell **115**(6):
738 727-738.
739 Kidd, A. R., 3rd, J. A. Miskowski, K. R. Siegfried, H. Sawa and J. Kimble (2005). "A beta-catenin identified
740 by functional rather than sequence criteria and its role in Wnt/MAPK signaling." Cell **121**(5): 761-772.
741 Lam, A. K. and B. T. Phillips (2017). "Wnt Signaling Polarizes C. elegans Asymmetric Cell Divisions During
742 Development." Results Probl Cell Differ **61**: 83-114.
743 Leduc, C., K. Padberg-Gehle, V. Varga, D. Helbing, S. Diez and J. Howard (2012). "Molecular crowding
744 creates traffic jams of kinesin motors on microtubules." Proceedings of the National Academy of
745 Sciences **109**(16): 6100-6105.
746 Leggett, D. S., J. Hanna, A. Borodovsky, B. Crosas, M. Schmidt, R. T. Baker, T. Walz, H. Ploegh and D.
747 Finley (2002). "Multiple associated proteins regulate proteasome structure and function." Mol Cell
748 **10**(3): 495-507.

749 Liu, W., X. Dong, M. Mai, R. S. Seelan, K. Taniguchi, K. K. Krishnadath, K. C. Halling, J. M. Cunningham, L.
750 A. Boardman, C. Qian, E. Christensen, S. S. Schmidt, P. C. Roche, D. I. Smith and S. N. Thibodeau (2000).
751 "Mutations in AXIN2 cause colorectal cancer with defective mismatch repair by activating beta-
752 catenin/TCF signalling." Nat Genet **26**(2): 146-147.
753 Mbom, B. C., K. A. Siemers, M. A. Ostrowski, W. J. Nelson and A. I. Barth (2014). "Nek2 phosphorylates
754 and stabilizes beta-catenin at mitotic centrosomes downstream of Plk1." Mol Biol Cell **25**(7): 977-991.
755 Mikenberg, I., D. Widera, A. Kaus, B. Kaltschmidt and C. Kaltschmidt (2007). "Transcription factor NF-
756 kappaB is transported to the nucleus via cytoplasmic dynein/dynactin motor complex in hippocampal
757 neurons." PLoS One **2**(7): e589.
758 Mila, D., A. Calderon, A. T. Baldwin, K. M. Moore, M. Watson, B. T. Phillips and A. P. Putzke (2015).
759 "Asymmetric Wnt Pathway Signaling Facilitates Stem Cell-Like Divisions via the Nonreceptor Tyrosine
760 Kinase FRK-1 in Caenorhabditis elegans." Genetics **201**(3): 1047-1060.
761 Miskowski, J., Y. Li and J. Kimble (2001). "The sys-1 gene and sexual dimorphism during gonadogenesis in
762 Caenorhabditis elegans." Dev Biol **230**(1): 61-73.
763 Mizumoto, K. and H. Sawa (2007). "Cortical beta-catenin and APC regulate asymmetric nuclear beta-
764 catenin localization during asymmetric cell division in C. elegans." Dev Cell **12**(2): 287-299.
765 Niehrs, C. and S. P. Acebron (2012). "Mitotic and mitogenic Wnt signalling." EMBO J **31**(12): 2705-2713.
766 Niehrs, C. and S. P. Acebron (2012). "Mitotic and mitogenic Wnt signalling." EMBO J **31**(12): 2705-2713.
767 Nusse, R. and H. Clevers (2017). "Wnt/beta-Catenin Signaling, Disease, and Emerging Therapeutic
768 Modalities." Cell **169**(6): 985-999.
769 O'Connell, K. F., C. Caron, K. R. Kopish, D. D. Hurd, K. J. Kemphues, Y. Li and J. G. White (2001). "The C.
770 elegans zyg-1 gene encodes a regulator of centrosome duplication with distinct maternal and paternal
771 roles in the embryo." Cell **105**(4): 547-558.

772 O'Rourke, S. M., M. D. Dorfman, J. C. Carter and B. Bowerman (2007). "Dynein modifiers in C. elegans:
773 light chains suppress conditional heavy chain mutants." PLoS Genet **3**(8): e128.
774 Peel, N., M. Dougherty, J. Goeres, Y. Liu and K. F. O'Connell (2012). "The C. elegans F-box proteins LIN-23
775 and SEL-10 antagonize centrosome duplication by regulating ZYG-1 levels." J Cell Sci **125**(Pt 15): 3535-
776 3544.
777 Peters, N., D. E. Perez, M. H. Song, Y. Liu, T. Muller-Reichert, C. Caron, K. J. Kemphues and K. F. O'Connell
778 (2010). "Control of mitotic and meiotic centriole duplication by the Plk4-related kinase ZYG-1." J Cell Sci
779 **123**(Pt 5): 795-805.
780 Phillips, B. T., A. R. Kidd, 3rd, R. King, J. Hardin and J. Kimble (2007). "Reciprocal asymmetry of SYS-
781 1/beta-catenin and POP-1/TCF controls asymmetric divisions in Caenorhabditis elegans." Proc Natl Acad
782 Sci U S A **104**(9): 3231-3236.
783 Pintard, L. and B. Bowerman (2019). "Mitotic Cell Division in Caenorhabditis elegans." Genetics **211**(1):
784 35-73.
785 Pinto, D., A. Gregorieff, H. Begthel and H. Clevers (2003). "Canonical Wnt signals are essential for
786 homeostasis of the intestinal epithelium." Genes Dev **17**(14): 1709-1713.
787 Priyanga, J., G. Guha and D. Bhakta-Guha (2021). "Microtubule motors in centrosome homeostasis: A
788 target for cancer therapy?" Biochim Biophys Acta Rev Cancer **1875**(2): 188524.
789 Reck-Peterson, S. L., W. B. Redwine, R. D. Vale and A. P. Carter (2018). "The cytoplasmic dynein
790 transport machinery and its many cargoes." Nat Rev Mol Cell Biol **19**(6): 382-398.
791 Reilein, A., D. Melamed, K. S. Park, A. Berg, E. Cimetta, N. Tandon, G. Vunjak-Novakovic, S. Finkelstein
792 and D. Kalderon (2017). "Alternative direct stem cell derivatives defined by stem cell location and
793 graded Wnt signalling." Nat Cell Biol **19**(5): 433-444.
794 Reya, T. and H. Clevers (2005). "Wnt signalling in stem cells and cancer." Nature **434**(7035): 843-850.

795 Sawa, H. (2012). "Control of cell polarity and asymmetric division in C. elegans." Curr Top Dev Biol **101**:
796 55-76.
797 Schlaitz, A. L., M. Srayko, A. Dammermann, S. Quintin, N. Wielsch, I. MacLeod, Q. de Robillard, A. Zinke,
798 J. R. Yates, 3rd, T. Müller-Reichert, A. Shevchenko, K. Oegema and A. A. Hyman (2007). "The C. elegans
799 RSA complex localizes protein phosphatase 2A to centrosomes and regulates mitotic spindle assembly."
800 Cell **128**(1): 115-127.
801 Schmidt, R., L. E. Fielmich, I. Grigoriev, E. A. Katrukha, A. Akhmanova and S. van den Heuvel (2017). "Two
802 populations of cytoplasmic dynein contribute to spindle positioning in C. elegans embryos." J Cell Biol
803 **216**(9): 2777-2793.
804 Shtutman, M., J. Zhurinsky, I. Simcha, C. Albanese, M. D'Amico, R. Pestell and A. Ben-Ze'ev (1999). "The
805 cyclin D1 gene is a target of the beta-catenin/LEF-1 pathway." Proc Natl Acad Sci U S A **96**(10): 5522-
806 5527.
807 Siegfried, K. R., A. R. Kidd, M. A. Chesney and J. Kimble (2004). "The sys-1 and sys-
808 3 Genes Cooperate With Wnt Signaling to Establish the Proximal-Distal Axis of the
809 Caenorhabditis elegans Gonad." Genetics **166**(1): 171-186.
810 Sonnichsen, B., L. B. Koski, A. Walsh, P. Marschall, B. Neumann, M. Brehm, A. M. Alleaume, J. Artelt, P.
811 Bettencourt, E. Cassin, M. Hewitson, C. Holz, M. Khan, S. Lazik, C. Martin, B. Nitzsche, M. Ruer, J.
812 Stamford, M. Winzi, R. Heinkel, M. Roder, J. Finell, H. Hantsch, S. J. Jones, M. Jones, F. Piano, K. C.
813 Gunsalus, K. Oegema, P. Gonczy, A. Coulson, A. A. Hyman and C. J. Echeverri (2005). "Full-genome RNAi
814 profiling of early embryogenesis in Caenorhabditis elegans." Nature **434**(7032): 462-469.
815 Sugioka, K., K. Mizumoto and H. Sawa (2011). "Wnt regulates spindle asymmetry to generate
816 asymmetric nuclear beta-catenin in C. elegans." Cell **146**(6): 942-954.
817 Sunchu, B. and C. Cabernard (2020). "Principles and mechanisms of asymmetric cell division."
818 Development **147**(13).

819 Tame, M. A., J. A. Raaijmakers, B. van den Broek, A. Lindqvist, K. Jalink and R. H. Medema (2014). "Astral
820 microtubules control redistribution of dynein at the cell cortex to facilitate spindle positioning." Cell
821 Cycle **13**(7): 1162-1170.
822 Tavernarakis, N., S. L. Wang, M. Dorovkov, A. Ryazanov and M. Driscoll (2000). "Heritable and inducible
823 genetic interference by double-stranded RNA encoded by transgenes." Nat Genet **24**(2): 180-183.
824 Tejpar, S., F. Nollet, C. Li, J. S. Wunder, G. Michils, P. dal Cin, E. Van Cutsem, B. Bapat, F. van Roy, J. J.
825 Cassiman and B. A. Alman (1999). "Predominance of beta-catenin mutations and beta-catenin
826 dysregulation in sporadic aggressive fibromatosis (desmoid tumor)." Oncogene **18**(47): 6615-6620.
827 Tetsu, O. and F. McCormick (1999). "Beta-catenin regulates expression of cyclin D1 in colon carcinoma
828 cells." Nature **398**(6726): 422-426.
829 Timmons, L. (2006). "Delivery methods for RNA interference in C. elegans." Methods Mol Biol **351**: 119-
830 125.
831 Valenzuela, J. I., M. Jaureguiberry-Bravo, D. A. Salas, O. A. Ramírez, V. H. Cornejo, H. E. Lu, T. A. Blanpied
832 and A. Couve (2014). "Transport along the dendritic endoplasmic reticulum mediates the trafficking of
833 GABAB receptors." J Cell Sci **127**(Pt 15): 3382-3395.
834 Vora, S. and B. T. Phillips (2015). "Centrosome-Associated Degradation Limits beta-Catenin Inheritance
835 by Daughter Cells after Asymmetric Division." Curr Biol **25**(8): 1005-1016.
836 Vora, S. M., J. S. Fassler and B. T. Phillips (2020). "Centrosomes are required for proper beta-catenin
837 processing and Wnt response." Mol Biol Cell **31**(17): 1951-1961.
838 Vora, S. M. and B. T. Phillips (2016). "The benefits of local depletion: The centrosome as a scaffold for
839 ubiquitin-proteasome-mediated degradation." Cell Cycle **15**(16): 2124-2134.
840 Wigley, W. C., R. P. Fabunmi, M. G. Lee, C. R. Marino, S. Muallem, G. N. DeMartino and P. J. Thomas
841 (1999). "Dynamic association of proteasomal machinery with the centrosome." J Cell Biol **145**(3): 481-
842 490.

843 Wójcik, C. and G. N. DeMartino (2003). "Intracellular localization of proteasomes." The International
844 Journal of Biochemistry & Cell Biology **35**(5): 579-589.
845 Wozniak, M. J., B. Bola, K. Brownhill, Y. C. Yang, V. Levakova and V. J. Allan (2009). "Role of kinesin-1 and
846 cytoplasmic dynein in endoplasmic reticulum movement in VERO cells." J Cell Sci **122**(Pt 12): 1979-1989.
847 Wühr, M., E. S. Tan, S. K. Parker, H. W. Detrich, 3rd and T. J. Mitchison (2010). "A model for cleavage
848 plane determination in early amphibian and fish embryos." Curr Biol **20**(22): 2040-2045.
849 Yang, L., X. Wu, Y. Wang, K. Zhang, J. Wu, Y. C. Yuan, X. Deng, L. Chen, C. C. Kim, S. Lau, G. Somlo and Y.
850 Yen (2011). "FZD7 has a critical role in cell proliferation in triple negative breast cancer." Oncogene
851 **30**(43): 4437-4446.
852 Zhunussova, G., G. Afonin, S. Abdikerim, A. Jumanov, A. Perfilyeva, D. Kaidarova and L. Djansugurova
853 (2019). "Mutation Spectrum of Cancer-Associated Genes in Patients With Early Onset of Colorectal
854 Cancer." Front Oncol **9**: 673.

855

856

857

858

859

860

861

862

863 **FIGURE LEGENDS**

864 **Figure 1:**

865 **Rationale and methodology for microtubule motor RNAi Screen.** A) GFP::SYS-1 can be occasionally
866 observed at regions corresponding to DHC-1 mitotic accumulation. This is particularly enhanced in
867 centrosomally uncoupled *rsa-2(RNAi)* embryos. The frequency of GFP::SYS-1 enrichment at these locales
868 in lacZ*(RNAi)* and rsa-2*(RNAi)* treatment is distinguished by color. A') GFP::SYS-1 at kinetochore
869 microtubule (white arrowhead) and cortex(black arrowhead) of the dividing *C. elegans* early embryo. B)
870 Demonstration of CEI and TEI calculation. CEI was calculated in FIJI by subtracting the mean pixel
871 intensity of a cytoplasmic ROI encompassing the proximal half of the dividing cell, approximated by the
872 light blue square, from a circular centrosome ROI, approximated by the white square. B') Expanded view
873 of ROI's as defined in B. B'') Graphical representation of the raw centrosomal and CEI adjusted
874 fluorescence intensity for the control (Left) and Affected (right) embryos in B. Control (*lacZ(RNAi)*
875 treated) exhibits both a high raw centrosomal GFP::SYS-1 and CEI. Affected (*rsa-2(RNAi)* treated) exhibits
876 an intermediate raw GFP::SYS-1, but severely decreased CEI, better reflecting its visual failure to
877 increase centrosomal GFP::SYS-1 notably above the bulk of cytoplasmic representation. C) Example
878 VENUS::SYS-1 CEI (C) and CEI/TEI (C') of controls and indicated dynein light chain depletions. Width of
879 the violin plot corresponds to a histogram of observation density. The median is indicated by the central
880 white dot, with the interquartile range indicated by the thick black line, and 1.5x additional Interquartile
881 range indicated by the thin black line. N= lacZ*(RNAi)*, 72; *dlc-1(RNAi),* 74; *dylt-1(RNAi),* 52; *rsa-2(RNAi)*,
882 22 * - $p<0.05$, ** - $p<0.01$, *** - $p<0.001$ by Chi-square test (A) or Student's t-test (C-C').

883 **Figure 2:**

884 **The dynein heavy chain Temperature Sensitive (dhc-1(ts)) Allele mediated loss of dynein function has**
885 **a disproportionate effect on SYS-1 localization**. A) Diagram of the Dynein motor, and hypothetical
886 model of its role in SYS-1 trafficking. Relative location of *dhc-1(ts)* lesion indicated. B) Representative
887 centrosome images of VENUS::SYS-1 and g-Tubulin::mCherry in wildtype and ts allele-containing
888 embryos C) embryos at comparable cell cycle phase before (top) and after (bottom) temperature
889 upshift. D) SYS-1 CEI and D') SYS-1 CEI per TEI in embryos containing *dhc-1(ts)* , to control for differences
890 in centrosome assembly, standard error depicted. N= 44, 31, 38, 25 in D and D' columns, left to right. * -
891 p<0.05, ** - p<0.01, *** - p<0.001 by Student's t-test.

892 **Figure 3:**

893 **Nocodazole mediated disruption of microtubules enhances centrosomal GFP::SYS-1 enrichment** A)
894 Representative images of GFP::TBB-1 in DMSO and Nocodazole treated embryos. White arrowheads
895 indicate astral microtubules (left) and the corresponding lack or dysregulated region in nocodazole
896 treatment (right) B) Quantification of, and C) Representative images of similarly treated GFP::SYS-1
897 embryos. For B, N=36 DMSO and 46 nocodazole treated embryos. * - p<0.05, ** - p<0.01, *** - p<0.001
898 by Student's t-test. D) CEI/TEI as evaluated with combinatorial Wildtype (WT) or *dhc-1(ts)* allele for
899 Dynein Heavy Chain, and treatment with 2% DMSO vehicle media or 2% DMSO + nocodazole media.
900 Measurements at the permissive and restrictive temperature are differentiated by blue and red
901 coloring, respectively. Error bars are SEM. E) Representative P_{sys-1}VENUS::SYS-1 and mCh::g-Tubulin for
902 each treatment in D, respectively.

903 **Figure 4:**

904 **Microtubule-mediated processes can also stabilize centrosomal SYS-1**. A) Treatment with *ecps-1(RNAi)*
905 enhances centrosomal SYS-1 accumulation, N=48 *lacZ(RNAi), N* =12 *rsa-2(RNAi), N*= 124 *ecps-1(RNAi).* B)

906 *lacZ(RNAi)* and *ecps-1(RNAi)* representative centrosomes in grayscale and intensity dependent LUT. C)
907 Putative dynein and proteasome adaptor ECPS-1 also appears to also enhance centrosomal ZYG-1
908 accumulation, by GFP::ZYG-1c CEI (N=31 untreated, N=19 *ecps-1(RNAi),* N= 20 *rpt-4(RNAi),* 14 *rsa-*
909 *2(RNAi)*) and D) Representative GFP::ZYG-1c centrosomal images in grayscale and intensity dependent
910 LUT. E) E) Quantified recovery of GFP::SYS-1. Values indicated are the ratio of bleached centrosomes to
911 their pre-bleach value, normalized such that the post-bleach value, t = 0, is 0 GFP::SYS-1 intensity. Error
912 bars are SEM. (F-F'') representative FRAP montage of 2nd division P1 cells in indicated embryos. Two
913 pre-bleach, immediately consecutive timepoints are followed by the 1st post-bleach image at time '0'
914 and images every 7 seconds thereafter indicated top left. * - p<0.05, ** - p<0.01, *** - p<0.001 by
915 Student's t-test. One-sided Student's T, asterisk indicates p-value from *lacZ(RNAi)* in E-F.

916 **Figure 5:**

917 **Effect of Dynein Depletion on nuclear SYS-1 Localization and Gene Expression in EMS Descendant**
918 **Cells**. A) The EMS precursor (embryo ventral cell) divides, receiving Wnt and Src specification and
919 orientation cues, respectively (red arrow). These daughters give rise to posterior, signaled E and
920 anterior, unsignaled MS daughter cells. Wildtype specification results in depicted approximate GFP::SYS-
921 1 localization pattern specifically enriched in the signaled daughter nucleus. B) Representative images of
922 wildtype and *ecps-1(RNAi)* treated embryos. Orange box encloses the unsignaled MS nucleus, Blue box
923 encloses the signaled E nucleus. C) Quantification of GFP::SYS-1 nuclear enrichment in indicated dynein
924 RNAi knockdowns. C') Mean difference in nuclear GFP::SYS-1 enrichment from quantification in C. Error
925 bars are SEM. D) Embryos ectopically expressing pEND-1::GFP::H2B in cells not descended from the E
926 lineage in the first (orange) second (blue) and third (green) lineage after the founding of the lineage (the
927 2, 4, and 8 cell E descendants, respectively). D') Representative embryos exhibiting WT (all lacZ*(RNAi)-*

928 treated, left) and ectopic (*ecps-1(RNAi)*- and 2x*dhc-1(RNAi)*- treated for 1, 2, and 3 generations after E
929 founding, respectively, right) pEND-1::GFP::H2B

930 **Figure 6:**

931 **SYS-1 dysregulation via dynein knockdown can cause rare distal tip cell fate conversions**. A) Diagram of
932 *C. elegans* distal tip cell signaled lineage specification in the somatic gonadal precursor. B)
933 Representative image of WT (top) and ectopically induced (bottom) distal tip cells (DTCs). To distinguish
934 DTC's from pLAG-2 driven vulval expression, DTCs are marked with white arrowheads. C) Number and
935 relative frequency of DTCs via anatomical marker in untreated animals and in backgrounds with RNAi
936 depletion of various dynein subunits. D) Number and relative frequency of DTCs marked by anatomical
937 marker when SYS-1 is overexpressed via a heat shock-driven transgene in both untreated animals and in
938 backgrounds with RNAi depletion of various dynein subunits. * = $p<0.05$, ** = $p<0.01$, *** = $p<0.001$ by
939 one-sided Mann-Whitney test

940 **Figure 7:**

941 **SYS-1 dysregulation via dynein knockdown can cause rare seam cell fate conversions.** A) Diagram of *C.*
942 *elegans* seam cell (SC) signaled lineage. B) Representative image of WT (top) and ectopically induced
943 (bottom) SCs. Likely ectopic SC exhibit spatially distinct 'doublets', highlighted here in brackets. C)
944 Number and relative frequency of SCs via anatomical marker when in untreated adults and in
945 backgrounds with RNAi depletion of various dynein subunits. D) Number and relative frequency of SCs
946 via anatomical marker when SYS-1 is overexpressed via a heat shock-driven transgene in both untreated
947 larvae and in backgrounds with RNAi depletion of various dynein subunits. * = $p<0.05$, ** = $p<0.01$, *** =
948 $p<0.001$ by Mann-Whitney test

949 **Figure 8:**

950 **Proposed model**. Speculation into the various processes by which SYS-1 and its regulators appear to be
951 localized to mitotic centrosomes. Both SYS-1 and some component of its centrosomal proteasome-
952 dependent negative regulators, here represented by purple circle, demonstrate some dependence on
953 microtubule mediated trafficking. While various dynein subunits are requisite components of a
954 functional dynein complex, the negative effect of their depletion on SYS-1 centrosomal steady state
955 indicates a preferential or more frequent trafficking of SYS-1. Relatively rare proteasome trafficking
956 events mediated by ECPS-1 meanwhile, are sufficient to maintain appropriate SYS-1 centrosomal
957 enrichment. This less efficient proteasomal trafficking, however, renders it vulnerable to Nocodazole-
958 mediated decrease in overall microtubule trafficking/network formation efficiency. Red inset depicts
959 decreased processivity or cargo binding capacity induced by dynein light chain RNAi depletions. Blue
960 inset depicts depletion of adapter ECPS-1 and resulting depletion of proteasome-trafficking specific
961 dynein complexes, while not otherwise affecting the microtubule motor.

962

963

964

965

966

967

968

969

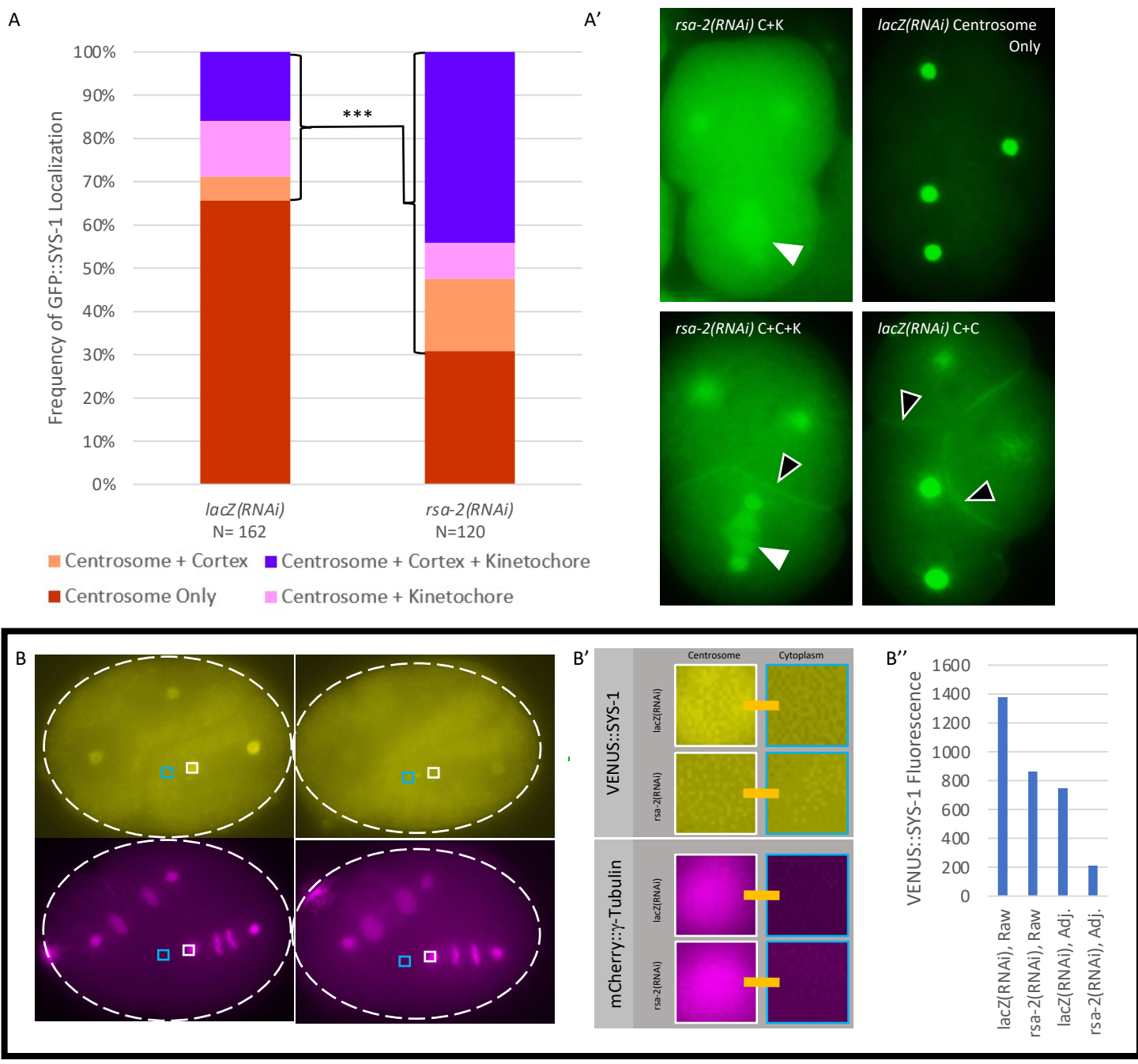
A
A'
Frequency of GFP::SYS-1 Localization
100%
90%
80%
70%
60%
50%
40%
30%
20%
10%
0%
***
lacZ(RNAi)
N= 162
rsa-2(RNAi)
N=120
Centrosome + Cortex
Centrosome + Cortex + Kinetochore
Centrosome Only
Centrosome + Kinetochore
rsa-2(RNAi) C+K
lacZ(RNAi) Centrosome Only
rsa-2(RNAi) C+C+K
lacZ(RNAi) C+C
B
B'
B''
VENUS::SYS-1
mCherry::γ-Tubulin
Centrosome
Cytoplasm
lacZ(RNAi)
rsa-2(RNAi)
VENUS::SYS-1 Fluorescence
1600
1400
1200
1000
800
600
400
200
0
lacZ(RNAi), Raw
rsa-2(RNAi), Raw
lacZ(RNAi), Adj.
rsa-2(RNAi), Adj.

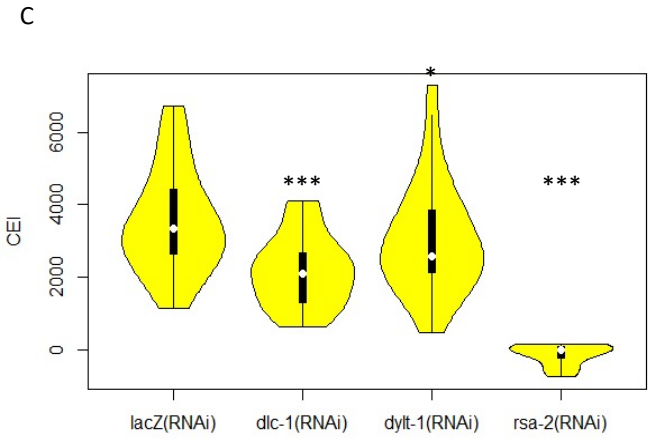
C
CEI
0
2000
4000
6000
*
***
***
lacZ(RNAi)
dlc-1(RNAi)
dylt-1(RNAi)
rsa-2(RNAi)

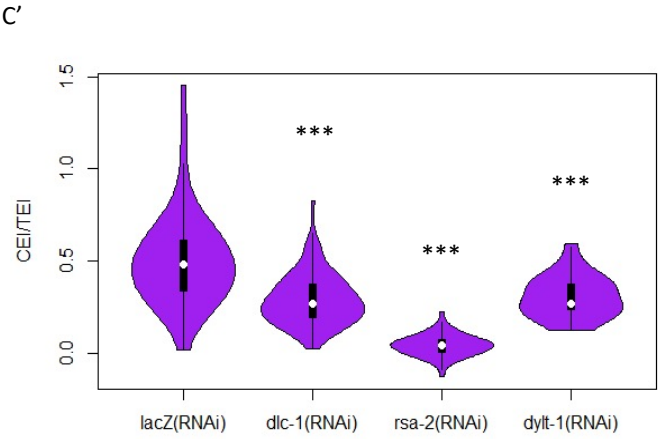
C'
CEI/TEI
0.0
0.5
1.0
1.5
***
***
***
lacZ(RNAi)
dlc-1(RNAi)
rsa-2(RNAi)
dylt-1(RNAi)

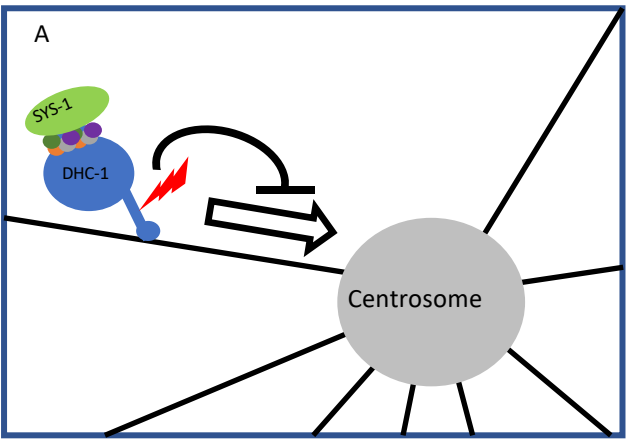
A
SYS-1
DHC-1
Centrosome

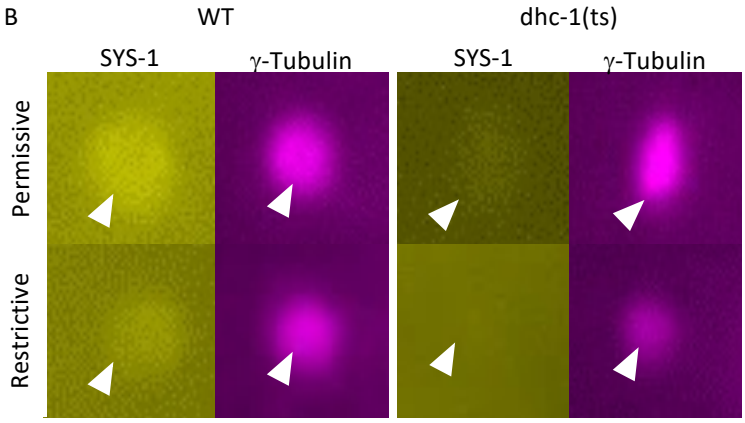
B
WT
dhc-1(ts)
SYS-1
γ-Tubulin
SYS-1
γ-Tubulin
Permissive
Restrictive

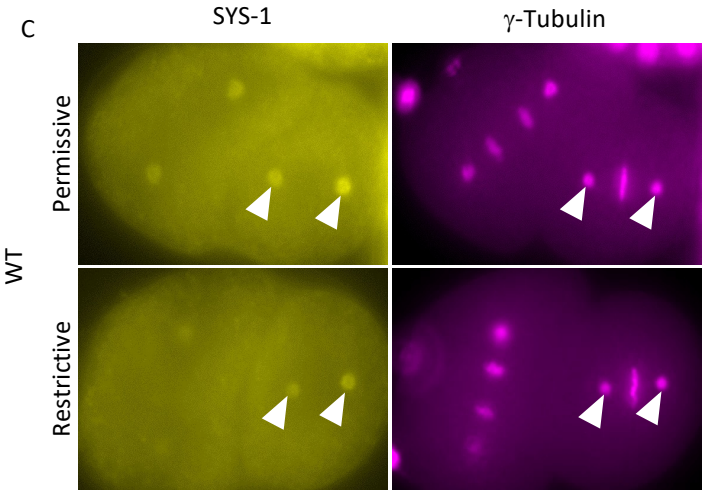
C
SYS-1
γ-Tubulin
WT
Permissive
Restrictive

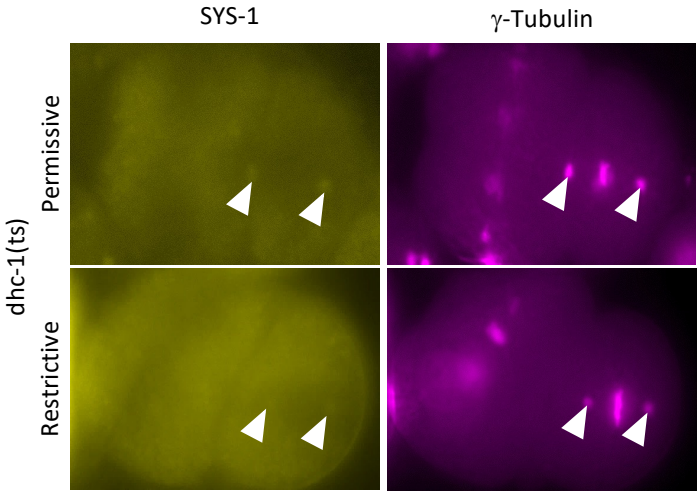
SYS-1
γ-Tubulin
dhc-1(ts)
Permissive
Restrictive

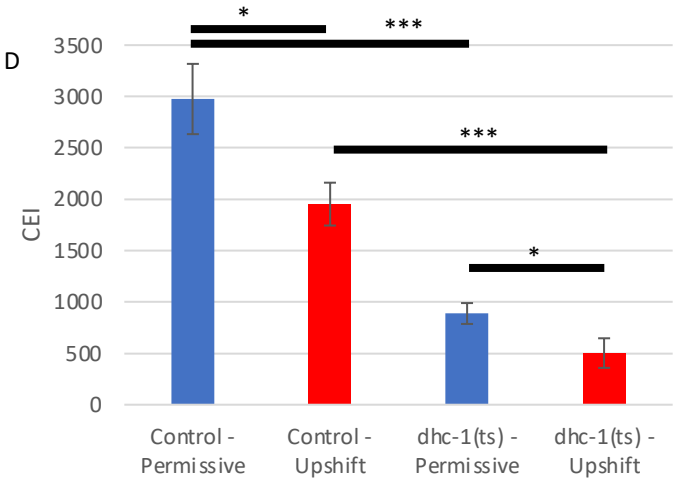
D
CEI
3500
3000
2500
2000
1500
1000
500
0
*
***
***
*
Control - Permissive
Control - Upshift
dhc-1(ts) - Permissive
dhc-1(ts) - Upshift

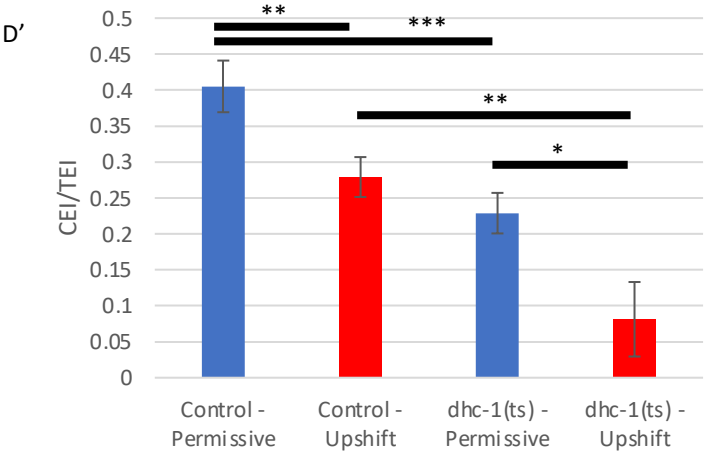
D'
CEI/TEI
0.5
0.45
0.4
0.35
0.3
0.25
0.2
0.15
0.1
0.05
0
**
***
**
*
Control - Permissive
Control - Upshift
dhc-1(ts) - Permissive
dhc-1(ts) - Upshift

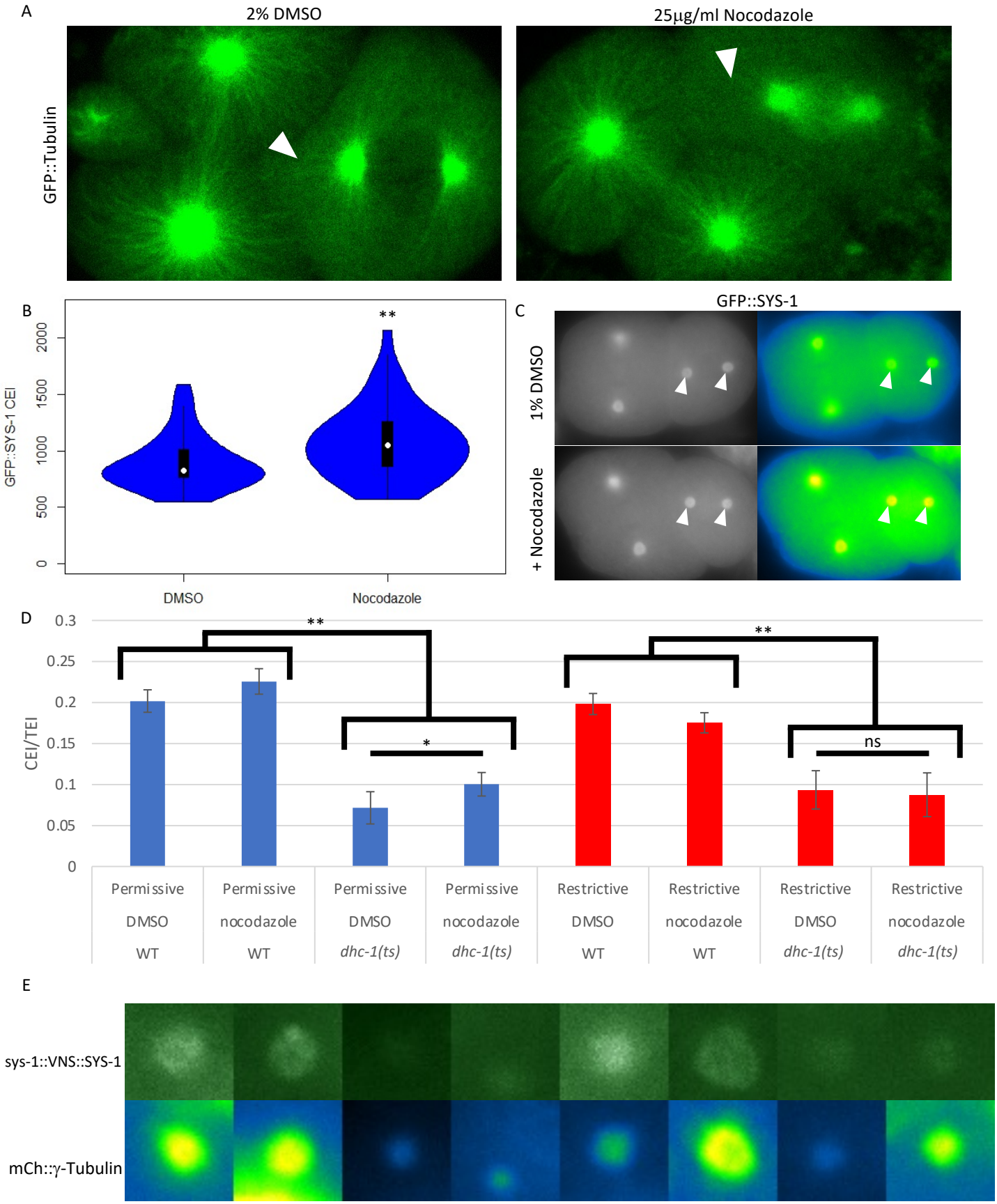
A
2% DMSO
25µg/ml Nocodazole
GFP::Tubulin
B
GFP::SYS-1 CEI
0
500
1000
1500
2000
**
DMSO
Nocodazole
C
GFP::SYS-1
1% DMSO
+ Nocodazole
D
CEI/TEI
0
0.05
0.1
0.15
0.2
0.25
0.3
**
*
**
ns
Permissive DMSO WT
Permissive nocodazole WT
Permissive DMSO dhc-1(ts)
Permissive nocodazole dhc-1(ts)
Restrictive DMSO WT
Restrictive nocodazole WT
Restrictive DMSO dhc-1(ts)
Restrictive nocodazole dhc-1(ts)
E
sys-1::VNS::SYS-1
mCh::γ-Tubulin

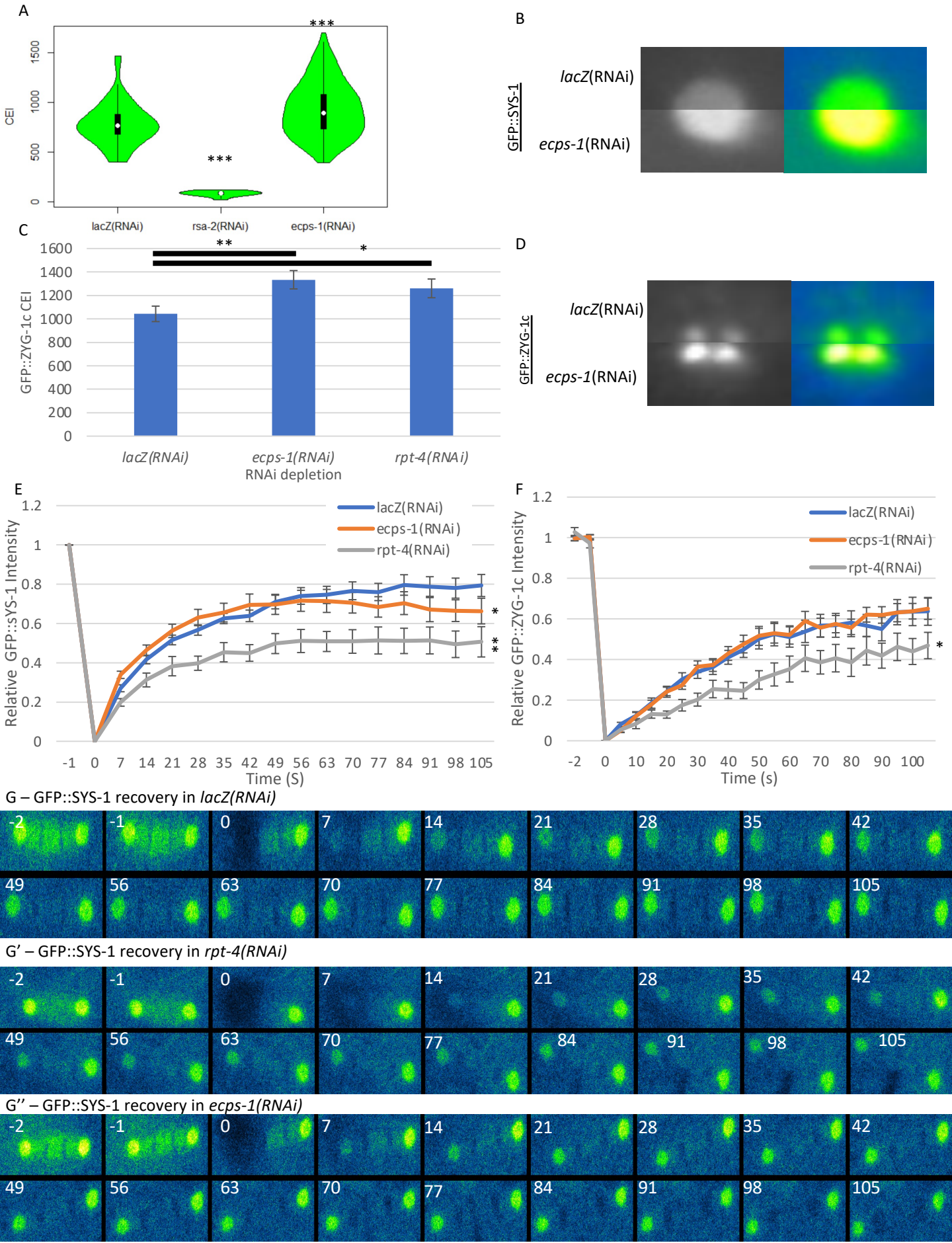
A
CEI
0
500
1000
1500
***
***
lacZ(RNAi)
rsa-2(RNAi)
ecps-1(RNAi)
B
GFP::SYS-1
lacZ(RNAi)
ecps-1(RNAi)
C
GFP::ZYG-1c CEI
0
200
400
600
800
1000
1200
1400
1600
**
*
lacZ(RNAi)
ecps-1(RNAi)
rpt-4(RNAi)
RNAi depletion
D
GFP::ZYG-1c
lacZ(RNAi)
ecps-1(RNAi)
E
Relative GFP::SYS-1 Intensity
0
0.2
0.4
0.6
0.8
1
1.2
lacZ(RNAi)
ecps-1(RNAi)
rpt-4(RNAi)
*
**
-1 0 7 14 21 28 35 42 49 56 63 70 77 84 91 98 105
Time (S)
F
Relative GFP::ZYG-1c Intensity
0
0.2
0.4
0.6
0.8
1
1.2
lacZ(RNAi)
ecps-1(RNAi)
rpt-4(RNAi)
*
-2 0 10 20 30 40 50 60 70 80 90 100
Time (s)
G – GFP::SYS-1 recovery in lacZ(RNAi)
-2 -1 0 7 14 21 28 35 42
49 56 63 70 77 84 91 98 105
G' – GFP::SYS-1 recovery in rpt-4(RNAi)
-2 -1 0 7 14 21 28 35 42
49 56 63 70 77 84 91 98 105
G'' – GFP::SYS-1 recovery in ecps-1(RNAi)
-2 -1 0 7 14 21 28 35 42
49 56 63 70 77 84 91 98 105

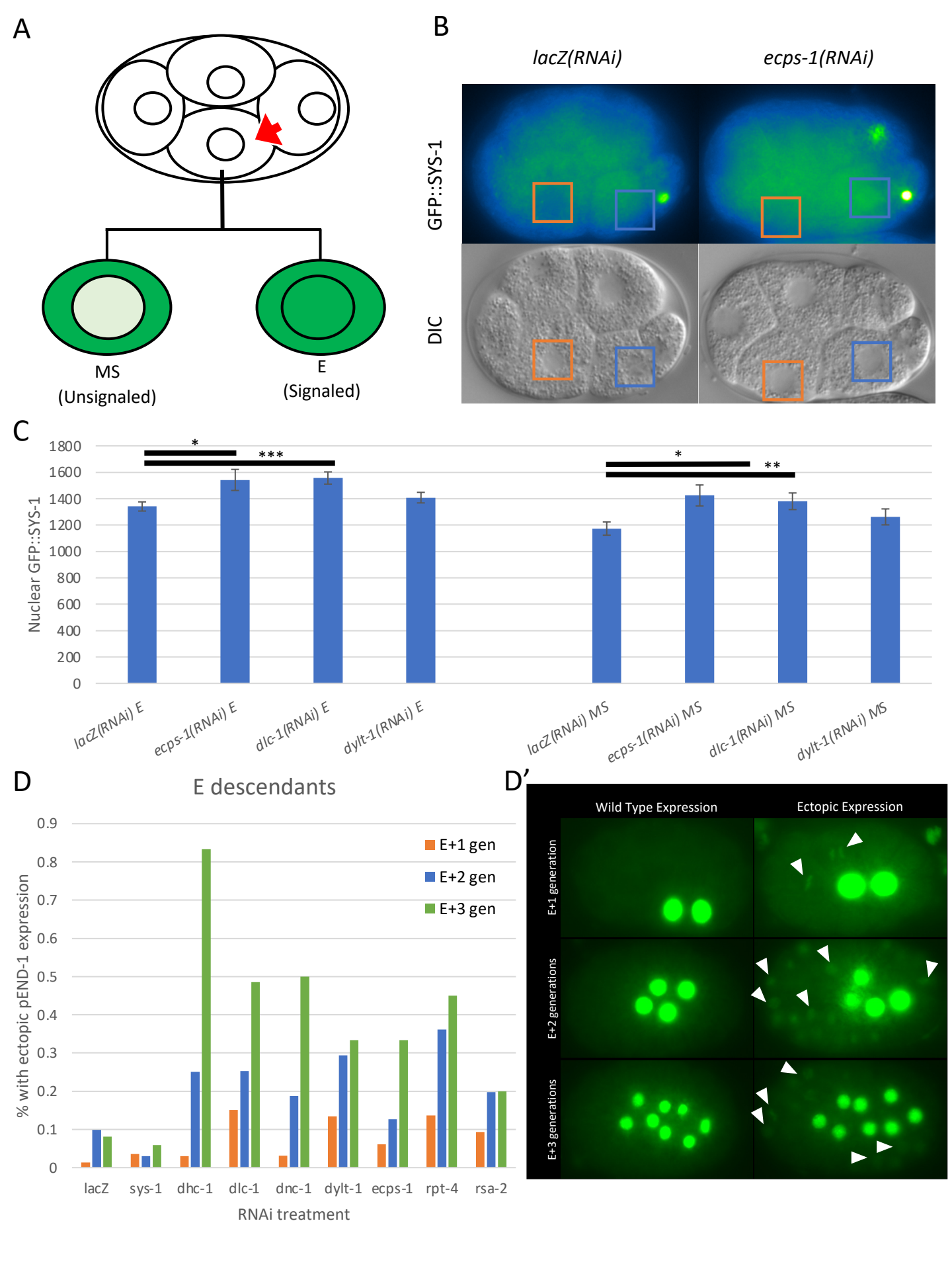
A
MS
(Unsignaled)
E
(Signaled)
B
lacZ(RNAi)
ecps-1(RNAi)
GFP::SYS-1
DIC
C
Nuclear GFP::SYS-1
1800
1600
1400
1200
1000
800
600
400
200
0
*
***
*
**
lacZ(RNAi) E
ecps-1(RNAi) E
dlc-1(RNAi) E
dylt-1(RNAi) E
lacZ(RNAi) MS
ecps-1(RNAi) MS
dlc-1(RNAi) MS
dylt-1(RNAi) MS
D
E descendants
% with ectopic pEND-1 expression
0.9
0.8
0.7
0.6
0.5
0.4
0.3
0.2
0.1
0
E+1 gen
E+2 gen
E+3 gen
lacZ
sys-1
dhc-1
dlc-1
dnc-1
dylt-1
ecps-1
rpt-4
rsa-2
RNAi treatment
D'
Wild Type Expression
Ectopic Expression
E+1 generation
E+2 generations
E+3 generations

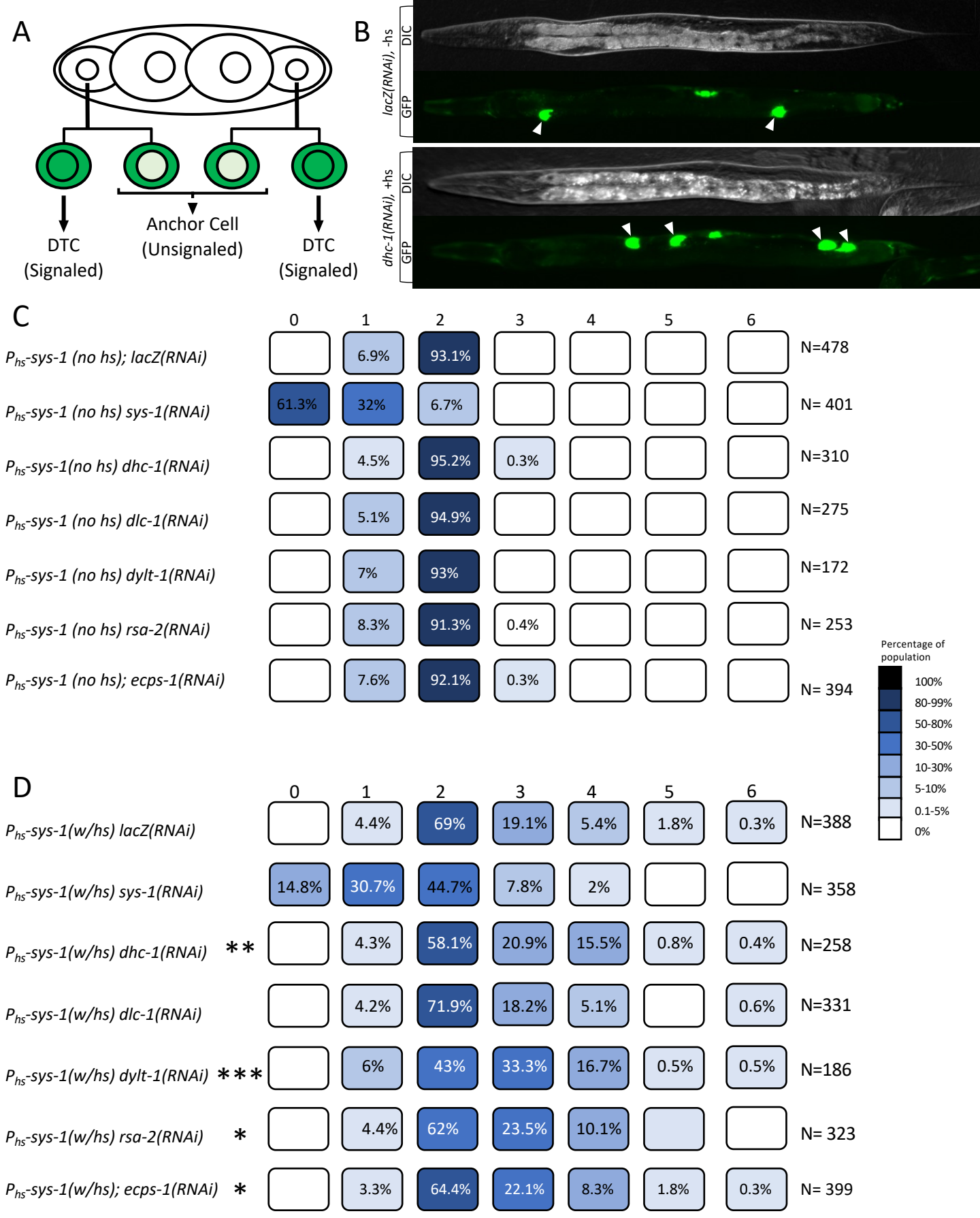
A
DTC
(Signaled)
Anchor Cell
(Unsignaled)
DTC
(Signaled)
B
lacZ(RNAi), -hs
DIC
GFP
dhc-1(RNAi), +hs
DIC
GFP
C
0 1 2 3 4 5 6
Phs-sys-1 (no hs); lacZ(RNAi) 6.9% 93.1% N=478
Phs-sys-1 (no hs) sys-1(RNAi) 61.3% 32% 6.7% N= 401
Phs-sys-1(no hs) dhc-1(RNAi) 4.5% 95.2% 0.3% N=310
Phs-sys-1 (no hs) dlc-1(RNAi) 5.1% 94.9% N=275
Phs-sys-1 (no hs) dylt-1(RNAi) 7% 93% N=172
Phs-sys-1 (no hs) rsa-2(RNAi) 8.3% 91.3% 0.4% N= 253
Phs-sys-1 (no hs); ecps-1(RNAi) 7.6% 92.1% 0.3% N= 394
Percentage of population
100%
80-99%
50-80%
30-50%
10-30%
5-10%
0.1-5%
0%
D
0 1 2 3 4 5 6
Phs-sys-1(w/hs) lacZ(RNAi) 4.4% 69% 19.1% 5.4% 1.8% 0.3% N=388
Phs-sys-1(w/hs) sys-1(RNAi) 14.8% 30.7% 44.7% 7.8% 2% N= 358
Phs-sys-1(w/hs) dhc-1(RNAi) ** 4.3% 58.1% 20.9% 15.5% 0.8% 0.4% N=258
Phs-sys-1(w/hs) dlc-1(RNAi) 4.2% 71.9% 18.2% 5.1% 0.6% N=331
Phs-sys-1(w/hs) dylt-1(RNAi) *** 6% 43% 33.3% 16.7% 0.5% 0.5% N=186
Phs-sys-1(w/hs) rsa-2(RNAi) * 4.4% 62% 23.5% 10.1% N= 323
Phs-sys-1(w/hs); ecps-1(RNAi) * 3.3% 64.4% 22.1% 8.3% 1.8% 0.3% N= 399

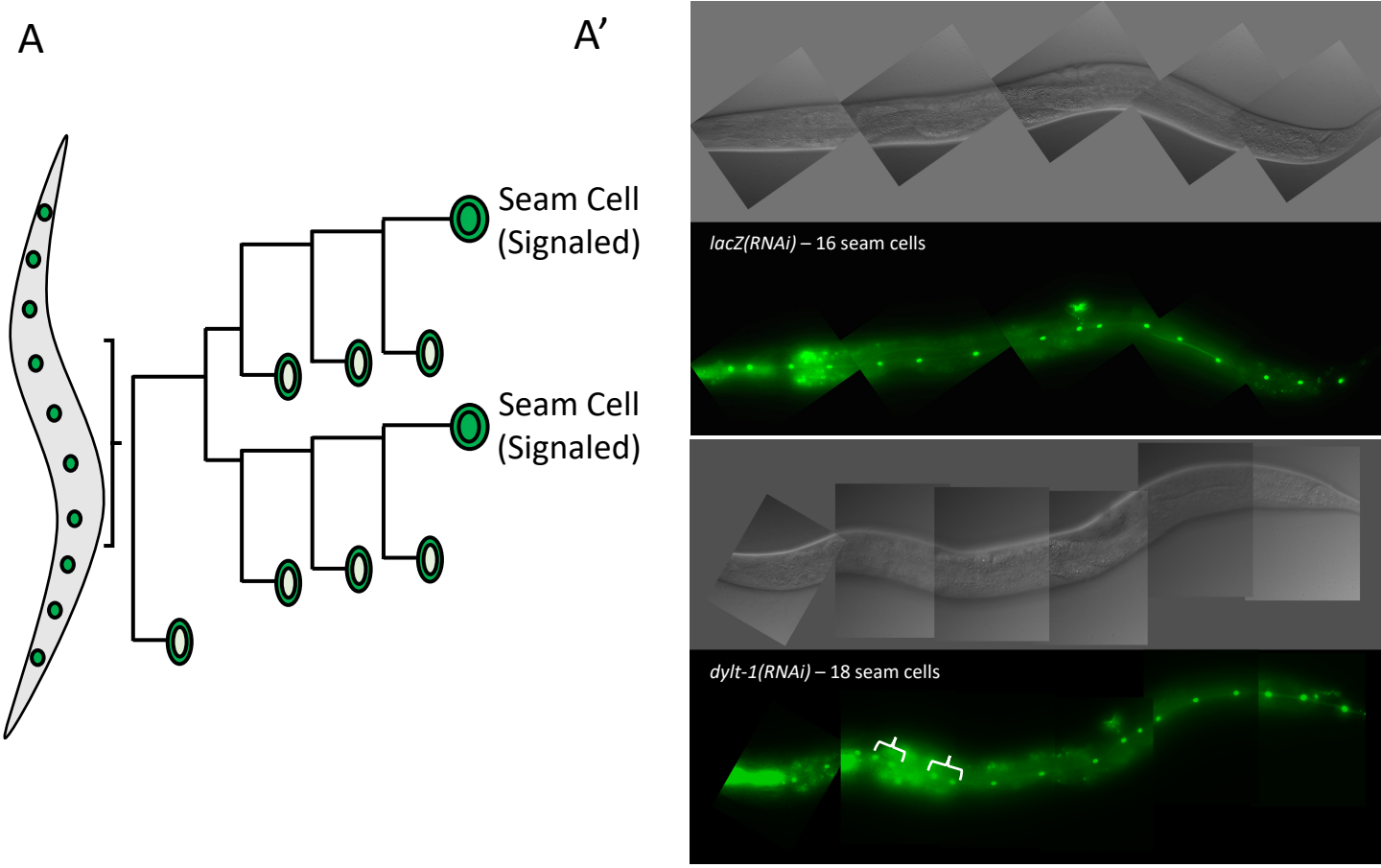

B

# of SCs		15	16	17	18	19	20	21	
P_{hs}-sys-1 (no hs); lacZ(RNAi)		1.7%	95%	3.3%					N=60
P_{hs}-sys-1 (no hs); dlc-1(RNAi)	*		90%	8.3%			1.7%		N= 60
P_{hs}-sys-1 (no hs); dylt-1(RNAi)	*		88.3%	10%			1.7%		N= 60

C

# of SCs		15	16	17	18	19	20	21	
P_{hs}-sys-1 (w/hs); lacZ(RNAi)		1.7%	80%	13.3%	5%				N=60
P_{hs}-sys-1 (w/hs); dlc-1(RNAi)	**	1.7%	58.3%	33.3%	5%	1.7%			N= 60
P_{hs}-sys-1 (w/hs); dylt-1(RNAi)	***	1.7%	38.2%	26.7%	11.7%	11.7%	5%	5%	N= 60

Percentage of population

- 100%
- 80-99%
- 50-80%
- 30-50%
- 10-30%
- 5-10%
- 0.1-5%
- 0%

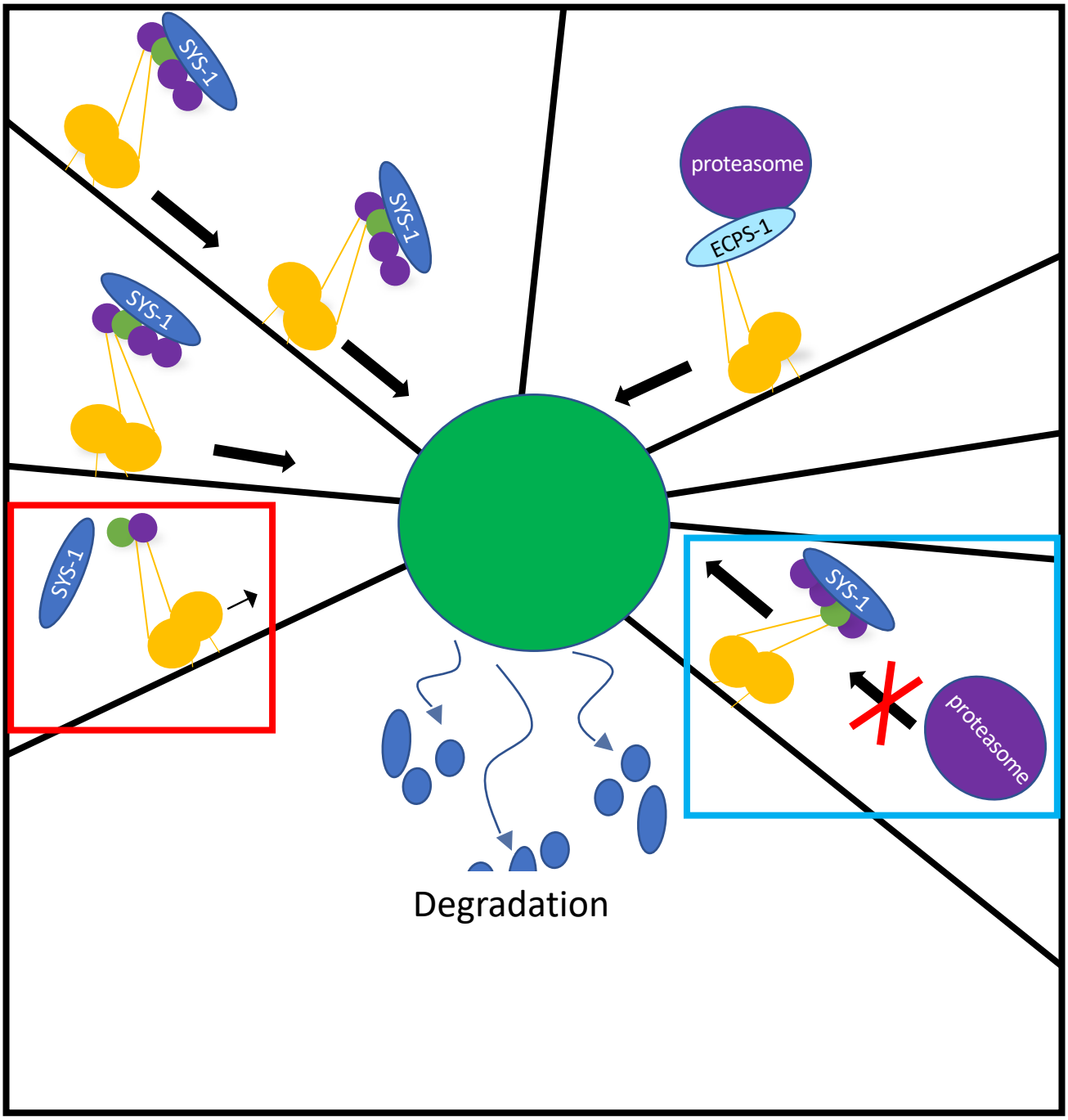
SYS-1
SYS-1
SYS-1
proteasome
ECPS-1
SYS-1
SYS-1
proteasome
Degradation